Fort Hays State University

FHSU Scholars Repository

Spring 2020

A Karst Feature Predictability Model within Barber County, Kansas

Gary M. Kelner
Fort Hays State University, gmkelner@mail.fhsu.edu

Follow this and additional works at: https://scholars.fhsu.edu/theses

 Part of the Geographic Information Sciences Commons, Geology Commons, and the Remote Sensing Commons

A KARST FEATURE PREDICTABILITY MODEL

WITHIN BARBER COUNTY, KANSAS

A Thesis Presented to the Graduate Faculty

of the Fort Hays State University in

Pa rtial Fulfillment of the Requirements for
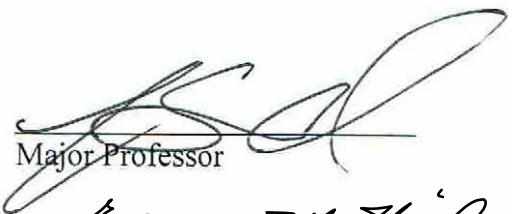
the Degree of Master of Science

by

Gary M. Kelner

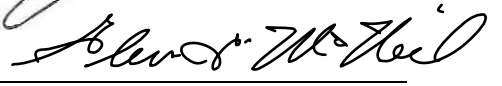B.S. Geology, University of Minnesota Duluth

Date ___April 8, 2020_____   Approved _____
                                            Major Professor

                                   Approved_____
                                            Graduate Dean

This thesis for

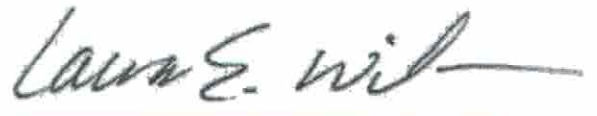the Master of Science Degree

By

Gary M. Kelner

has been approved

_____

Dr. Jonathan Sumrall, Committee Chair

_____

Dr. Keith Bremer, Committee Member

_____

Dr. Richard Lisichenko, Committee Member

_____

Chair, Department of Geosciences

i

ABSTRACT

This research consisted of two topics: 1) geographic predictive models of karst features and 2), a petrographic study examining the lithology of the study area. The study area is a privately owned ranch in the Gypsum Hills of Barber County, Kansas and is known to have karst features. Two predictive models for karst features were utilized. Previously identified features, Light Detection and Ranging (LiDAR), and Advanced Spaceborne Thermal Emission and Reflection Radiometer (ASTER) imagery aided in the creation of these predictive models. These predictability models also used the ESRI ArcMap software platform. The data for these models consists of slope, aspect, nearest neighbor elevation, Normalized Difference Vegetation Index (NDVI), land cover/land use, distance to geomorphic features, surface geology, and other attributes calculated in ArcMap. Other software platforms were also used in the creation of these models (Microcomputer Digital Elevation Models (MicroDEM), System for Automated Geoscientific Analyses (SAGA) GIS and Environment for Visualizing Images (ENVI) for imagery analysis). To test these models, features were identified using the sink-fill function in ArcMap on hillshade layers generated from LiDAR data. Field validation of these models successfully identified 52% of the validation points as having karst features, as well as 12 additional points in high probability areas that were visited. A total of 38 additional points (a 51% increase in the karst database) were added to the karst inventory for the property. Understanding the distribution and occurrence of karst features will help landowners mitigate risk such as collapse leading to structural damage and aquifer contamination. Although this model focused on Barber County, Kansas, the techniques and approaches used by these two models may be useful in creating future predictive models in other karst areas.

The petrographic portion of this research identified two geologic sedimentary facies using petrographic thin sections from various karst features. The two facies were: 1) Algal Mat and 2) Peloidal. These facies are very close to one another spatially when plotted by sample location within the property. The relative elevation of these facies places the Algal Mat facies below the Peloidal facies. This suggests that there are multiple facies that control karst feature formation as opposed to only the basal carbonates suggested by previous studies.

ACKNOWLEDGEMENTS

I would like to thank my advisor Dr. Jonathan Sumrall for his advice and guidance throughout this thesis and my graduate school education. I want to thank you for making me a better student as well as scientist and for all of your advice and assistance throughout my time at Fort Hays State University in the Geosciences Department.

My extreme gratitude goes to Dr. Keith Bremer for his assistance with this thesis and making me a better writer and public speaker, to this I cannot say thank you enough. To Dr. Richard Lisichenko, I cannot express how grateful I am to you for all of your help with the GIS analyses conducted for this thesis as well as making me a better person.

I wish to extend many thanks to the ranch owners Mr. and Mrs. Hinz for their willingness to grant me access to their land for research and sample collection. I could not have completed this thesis without their cooperation.

Many thanks to Jonathan Camelo, Kaitlyn Gauvey, and Alex Lyles. Thank you very much for your assistance with the collection of field data for this project as well as advice and guidance on the creation of the petrographic thin sections and completion of this thesis.

A special thank you to my parents Bill and Lori Kelner, siblings Joe and Lauren Kelner, aunts, uncles, grandparents, cousins, friends, and colleagues for their encouragement and support throughout my graduate school education and completion of this thesis. I could not have done it without you.

TABLE OF CONTENTS

LIST OF FIGURES

LIST OF TABLES

LIST OF EQUATIONS

LIST OF APPENDICIES

CHAPTER I

INTRODUCTION

1.1   Chapter Overview

This chapter presents the goals and hypotheses of this project. In addition, there is

a short discussion of terminology used throughout this thesis, especially covering basic

data types used in Geographic Information Systems (GIS).

1.2   Introduction

Karst features are numerous within Barber County, Kansas and being able to

predict their location can be very beneficial for landowners and environmental

organizations alike. The Gypsum Hills of Barber County, Kansas hosts a variety of karst

features (Gauvey, 2019). The goals of this project are to: 1) create a predictive model for

karst features using Geographic Information Systems (GIS) and remote sensing, 2) create

a karst hazard map using GIS and the predictive model, and 3) refine the geologic

constraints that lead to karst formation in the study area. For the predictive model

creation, it is hypothesized that specific mappable landscape attributes (ex. surface

drainage, elevation, geology, etc.) lead to the formation of karst features in Barber

County, and these attributes can be used to create an accurate predictive model of where

karst features occur in the study area. Furthermore, understanding the localized geologic

variations will assist in the creation of future models in the region.

Understanding the distribution and occurrence of karst features will help

landowners mitigate risk (e.g. collapse leading to structural damage, dam failures, and

aquifer contamination). The karst predictive model will also be useful for future

exploration of features in Barber County, such as caves, which may contain rare or threatened organisms. This predictive model may also be modified for other gypsum areas of the world as a preliminary analysis tool for identification of karst features. It is hypothesized that the predictive model will more accurately identify the location of unknown karst features compared to simply using the sink-fill function within ArcMap. Additionally, it is hypothesized that karst features are associated with areas of high vegetation index, which correlates to a higher amount of water present.

The geologic controls on karst formation have been documented on this property and within Barber County (Gauvey, 2019; Young and Beard, 1993). These geologic controls include structural features (joint and faults) and stratigraphic features (mixed carbonates and evaporite layers that dissolve at differing rates) (Gauvey, 2019). The previous investigation on this property identified an important stratigraphic layer that was present in all caves and within all sinkholes (Gauvey, 2019); however, detailed petrology and stratigraphic investigations were not conducted to be able to discern if a single layer is present or if multiple layers are present. The second component of this thesis addresses this issue. It is hypothesized that a single carbonate unit within the stratigraphy of the property exists that controls the formation of karst features. This single carbonate unit is less soluble than the overlying gypsum and displays a relatively consistent petrographic composition. To address this component of the thesis, sedimentary facies will be determined from petrographic analyses to evaluate the depositional environment. The presence of a single sedimentary facies will confirm the petrologic hypothesis stated above.

GIS and Remote Sensing Terminology:

- **Geographic Information System (GIS)** - a collection of computer software used to manage and analyze information about geographic places, spatial relationships and spatial processes (Wade and Sommer, 2006).

- **Vector data** - geometric features that have both spatial and non-spatial attributes. Vector data is defined as a data model that is coordinate based and represents point, line, and polygon features within a geographic space (Wade and Sommer, 2006). Vector data features are generally simple to visualize and represent consistent features or values on the landscape. Vector functions include: buffers, intersects, Euclidean distance, merge, and others.

- **Raster data** - a spatial data model that is made up of single or multiple bands that consist of cells that are arranged in a grid pattern or matrix (Wade and Sommer, 2006). Individual cell sizes represent the resolution of the raster data (example: 30-meter cell size represents 30-meter resolution). The resolution of the raster data determines the size of the geographic features that can be represented. Each cell has a location and attribute value, and groups of cells that share the same values represent the same geographic feature. Raster functions operate on raster data to summarize or assist in other calculations.

- **Coordinate System** - a method for identifying a location of a point on the surface of the earth.

- **Geographic projection** - the systematic distortion necessary to portray the curved surface of the earth on a flat map.

- **ArcGIS** - a computer software platform that allows for the analysis, curation and visualization of geographic information which is usually in a map.

- **ArcMap** - a subset of the larger computer software platform ArcGIS that specifically allows for map creation and dissemination.

- **Buffer** - an area defined by a specific distance around a vector feature.

- **Digital Elevation Model (DEM)** - a model of the 3D landscape in a raster file format.

- **Slope** - the relative angle of tilt of the land surface with each raster cell size. Instead of displaying elevation like the DEM, slope maps have a value field of slope (in degrees).

- **Aspect** - the direction that the slope is facing and is given in degrees from zero to 360 and compass direction (Wade and Sommer, 2006). This is an important calculation because it can identify slopes that receive more sunlight (southern facing in the northern hemisphere) among other uses for aspect.

- **Light Detection And Ranging (LiDAR)** - LiDAR uses the distance that a laser travels from its source to the surface of the earth. The resulting distance is what show the topography of the earth.

- **Advanced Spaceborne Thermal Emission Reflection Radiometer (ASTER)** - a spacecraft that collects imagery in multiple bands of light which allows for a multitude of spatial analyses.

Geologic Terminology:

- **Sedimentary Facies** – a packet of sedimentary rock that has characteristics that distinguish it from other packets of sedimentary rock (Tucker, 2009).

- **Petrographic Thin Section** - a microscope slide with a thin slice of rock adhered to it and thin enough for light to pass through.

- **Allochem** - a recognizable grain when viewing sedimentary rocks. An example would be fossils.

- **Petrography** - the analysis of rocks underneath a microscope to determine their composition and microscopic characteristics.

- **Plane Polarized Light** - the waves of light are all vibrating in the same direction and are parallel.

- **Cross Polarized Light** - the waves of light are vibrating in perpendicular directions.

- **Karst** - a landscape that develops on soluble rocks (White, 1988; Ford and Williams, 1989; Palmer, 2007).

- **Cave -** a feature that is large enough to admit a human (Palmer, 2007).

- **Sinkhole -** a surface geomorphic feature that results from the collapse of the surface material (Palmer, 2007).

- **Epikarst** - a solutionally enlarged opening that is also characterized as shallow surficial karst.

- **Swallow Hole** - a visible opening that acts as an insurgence point for water to enter the subsurface through fractures or joints.

- **Speleogenesis** - the study of the formation and origin of caves (White, 1988; Ford and Williams, 1989; Palmer, 2007).

CHAPTER II

GEOGRAPHIC AND GEOLOGIC SETTING

2.1   Chapter Overview

The landscape of Barber County is described in this chapter. Specific geographic features are outlined and the bedrock geology is described in detail. This section has been separated from the Literature Review (Chapter IV) because this represents fundamental geoscience background required for any study conducted in Barber County, Kansas. The Literature Review chapter is specific to methods and studies that this thesis is built upon.

2.2   Physiography of the Study Area

Barber County is located in southcentral Kansas (Figure 1). The landscape of Barber County is rugged and heavily influenced by the rivers and water features within the area (Figure 2). There are buttes and mesas that can be seen throughout the area, which are formed by resistant layers within the Medicine Lodge Gypsum (Benison et al., 2015). The area also contains a large amount of valleys (large valleys are locally referred to as draws, and small valleys are locally referred to as washes) that are formed by the erosion caused by water flowing through the area.
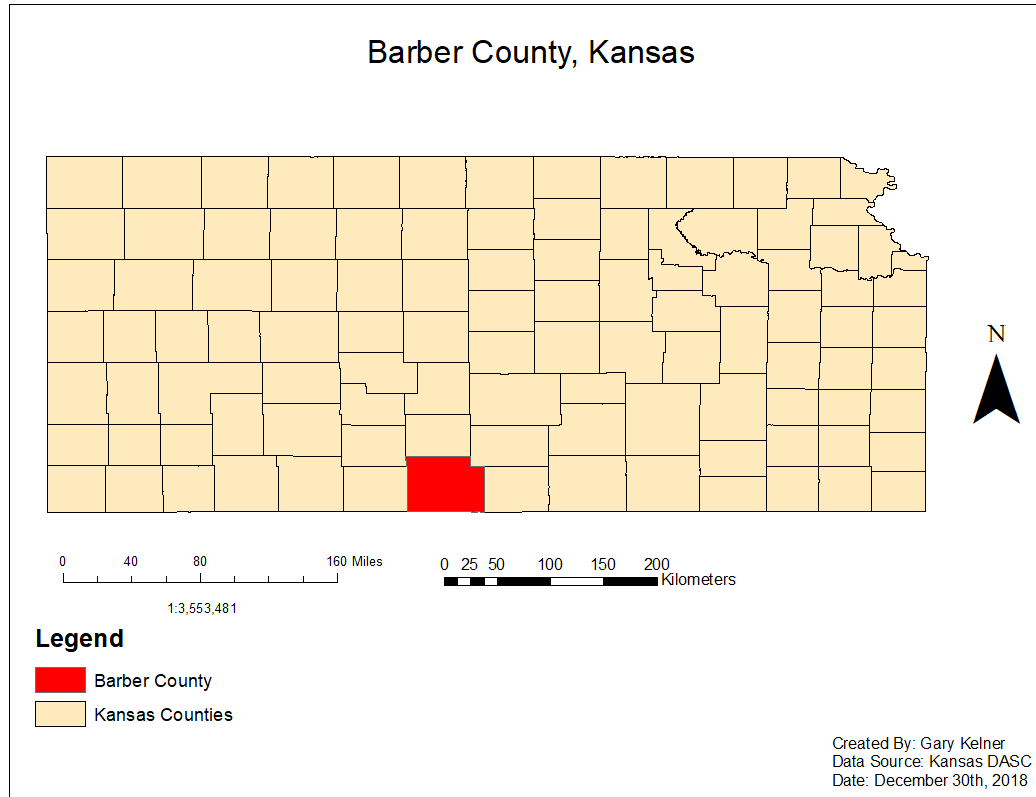
Figure 1. Barber County's location within the state of Kansas. Barber County is located in southcentral Kansas along the Kansas Oklahoma border.

A single ranch approximately 4,000 acres in size is the study location (Figure 3). Much of the study area is used as rangeland and leased for livestock grazing and hunting use during the applicable seasons throughout the year. The use of the landscape by livestock creates animal trails which creates useful navigation paths that aid in negotiating the steep draws and washes that are common throughout the area. This single property was used instead of the entire county due to time constraints for field validation.
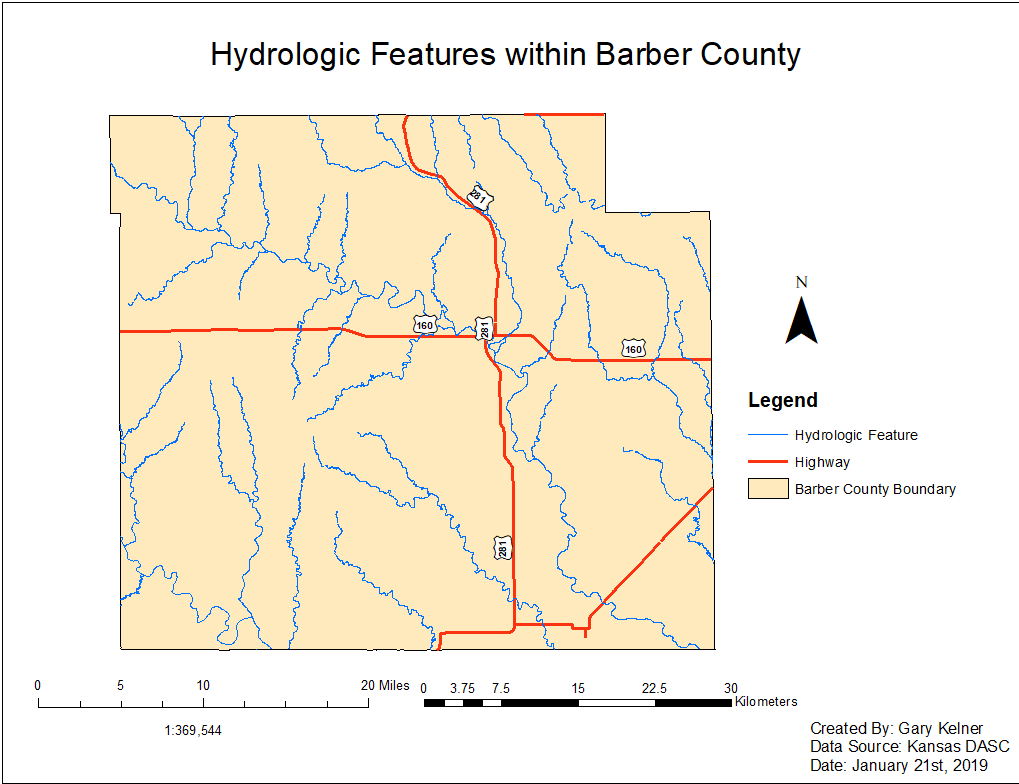
Figure 2. Hydrologic Features within Barber County Map
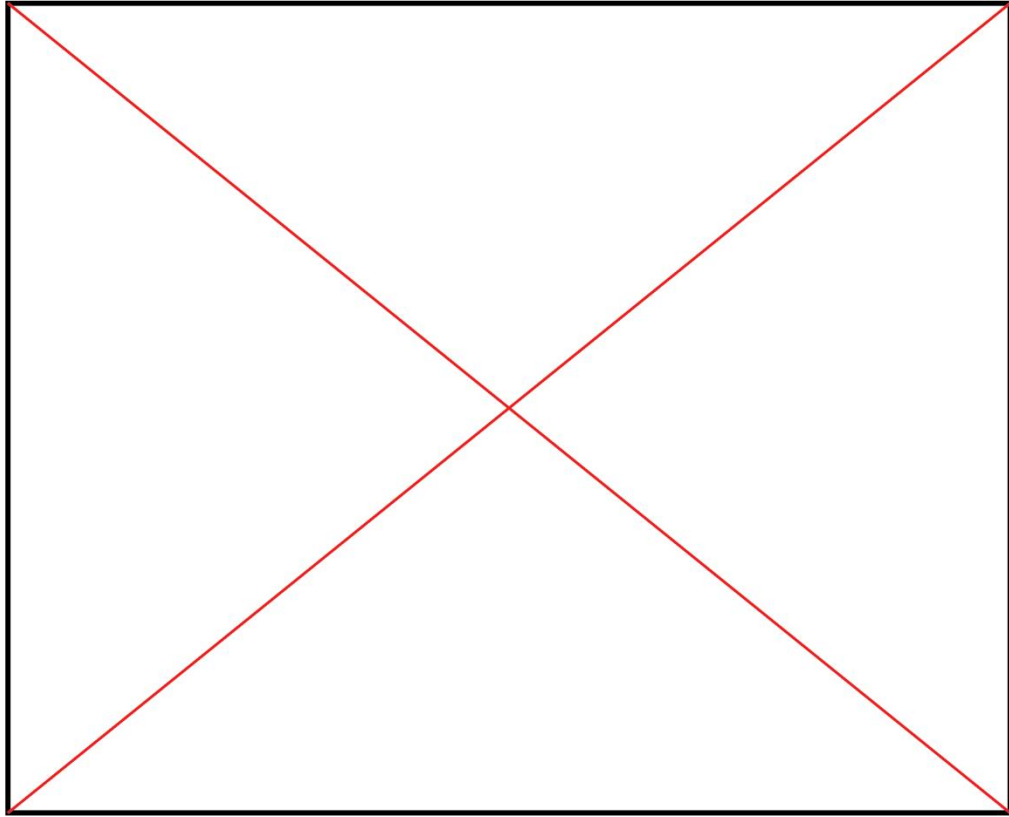
Figure 3. An outline of the property's location within Barber County.

2.3   Background Geology of the Study Area

The geology of Barber County, Kansas is dominated by sedimentary deposits that are part of the Permian System (Figure 3). These Permian deposits are found in the subsurface throughout most of Kansas (Figure 4). Permian red beds and evaporites are found extensively throughout the middle of the North American continent. These sediments that make up the red beds and evaporites were deposited in the Permian Basin approximately 276 million years ago (Benison et al., 2015). The study area's geology was influenced by the Las Animas Arch to the west and the Nemaha Anticline to the east

(Figure 5). These tectonic features contributed to the structures and orientations of strata

observed in Barber County, Kansas.
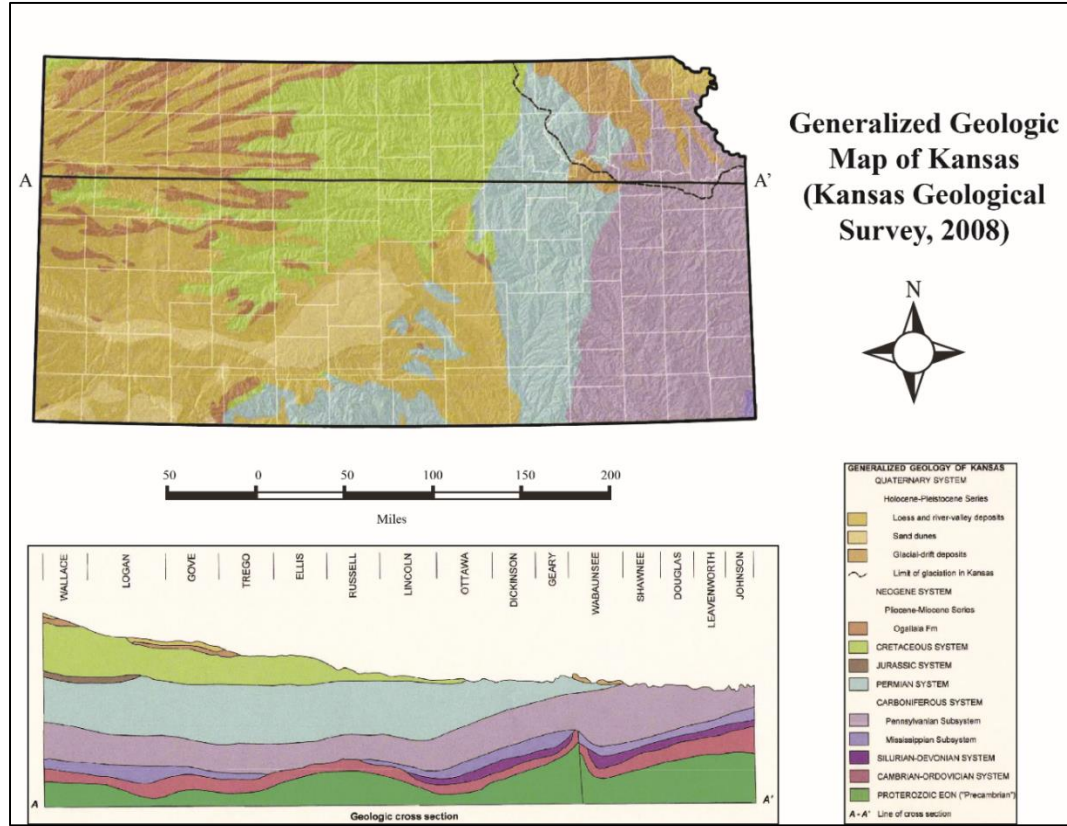
Figure 4. Generalized geologic map and cross section of the state of Kansas. The Permian System is colored light blue and is found in the subsurface in the majority of central to western Kansas.
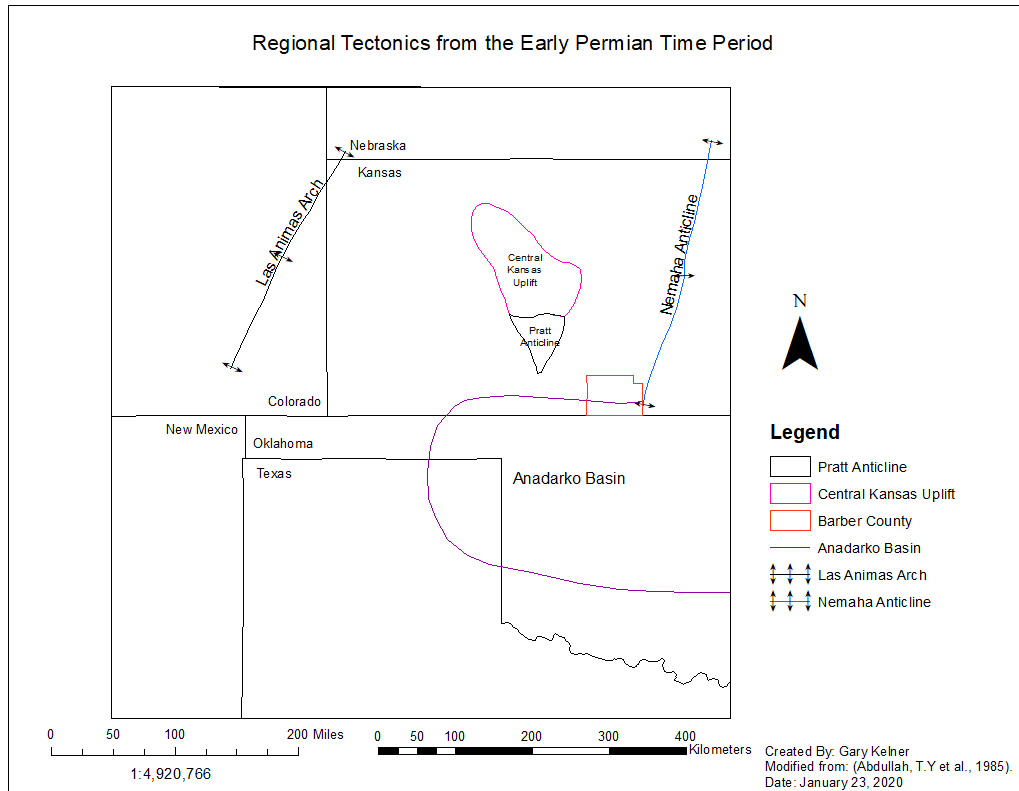
Figure 5. The Early Permian tectonic features surrounding the study (Modified from Abdullah et al., 1985).

The stratigraphy of Barber County, Kansas is dominated by the Permian Nippewalla Group (Figure 6). These red bed–evaporite sequences were classified in the late 1800's (Cragin, 1896) and further refined into individual units during the 1930's (Norton, 1939). Further outcrop and subsurface studies on this stratigraphy in Kansas and Oklahoma include: Kulstad et al. (1956), Ham (1960), Fay, (1964), and Johnson (1967). Petrography of the sediments of the Nippewalla Group in southcentral Kansas was described by Swineford (1955) and Benison et al., (2015).
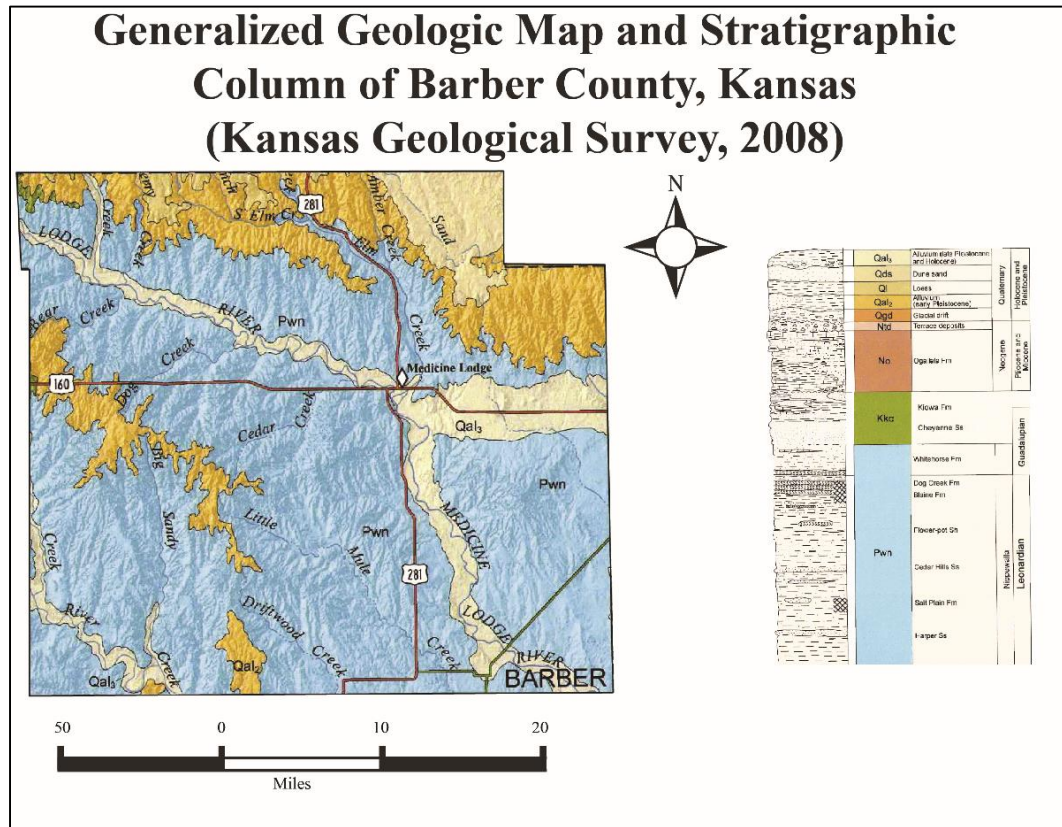
Figure 6. The generalized geologic map and stratigraphic column for Barber County, Kansas.

The Nippewalla Group consists mostly of red beds that were deposited on a broad, flat, arid alluvial-aeolian plain bordering a shallow inland sea (Hills, 1942; Swineford, 1955). The group is primarily composed of siltstones and very fine-grained sandstones, with minor amounts of silty shale and rock gypsum. The Nippewalla Group is divided into six formations (from bottom to top): Harper Sandstone, Salt Plain Formation, Cedar Hills Sandstone, Flowerpot Shale, Blaine Formation, and Dog Creek Shale. The Dog Creek Shale is commonly grouped with the Blaine formation, as it lies between the uppermost gypsum of the Blaine and the base of the Whitehorse sandstone.

The Blaine Formation, above the Flowerpot Shale, is part of the Nippewalla Group (Benison et al., 2015; Benison and Goldstein, 2001). The Blaine Formation forms the cap-rocks of the buttes seen in Barber County, Kansas (Benison et al., 2015). The Blaine Formation located within Barber County Kansas was deposited in a shallow lake environment (Benison et al., 2015). The bedded anhydrite facies within the Nippewalla Group does not contain any carbonate minerals and represents deposition in a saline lake environment (Benison and Goldstein, 2001). The depositional environment of the area of study was interpreted as an arid saline/hypersaline lacustrine (lake) environment that fluctuated between halite and gypsum as the water levels varied during the Permian (Benison et al., 2015).

The Blaine Formation is exposed in Barber, Comanche, and Kiowa counties. The Blaine Formation is divided into four members: Haskew Gypsum, Shimer Gypsum, Nescatunga Gypsum, and the Medicine Lodge Gypsum (Norton, 1939). The Haskew Gypsum, upper member of the Blaine Formation, consists of less than one foot of gypsum underlain by about five feet of brown-red shale (Moore et al., 1951). The Shimer Gypsum underlies the Haskew member and consists of a 13–23 feet bed of massive gypsum overlying approximately one foot of dolomite (Moore et al., 1951). The Nescatunga Gypsum includes about eight feet of red shale overlying five feet (1.5 m) of gypsum, and eight feet of red shale underlying the gypsum (Moore et al., 1951). The Medicine Lodge Gypsum, lowest in the stratigraphic section, is the thickest bed of gypsum in Kansas, measuring up to more than 30 feet (Moore et al., 1951). The Medicine Lodge Gypsum grades into a foot of oolitic/pellitic dolomite called the Cedar Springs Dolomite (Fay, 1964). Below the Medicine Lodge Gypsum is the Flowerpot Shale

Formation. Barber County, Kansas is known for containing a large number of karst features (Figure 7), and previous work has suggested a petrographic control of the Cedar Springs Dolomite on the development of karst in this region (Gauvey and Sumrall, 2018).
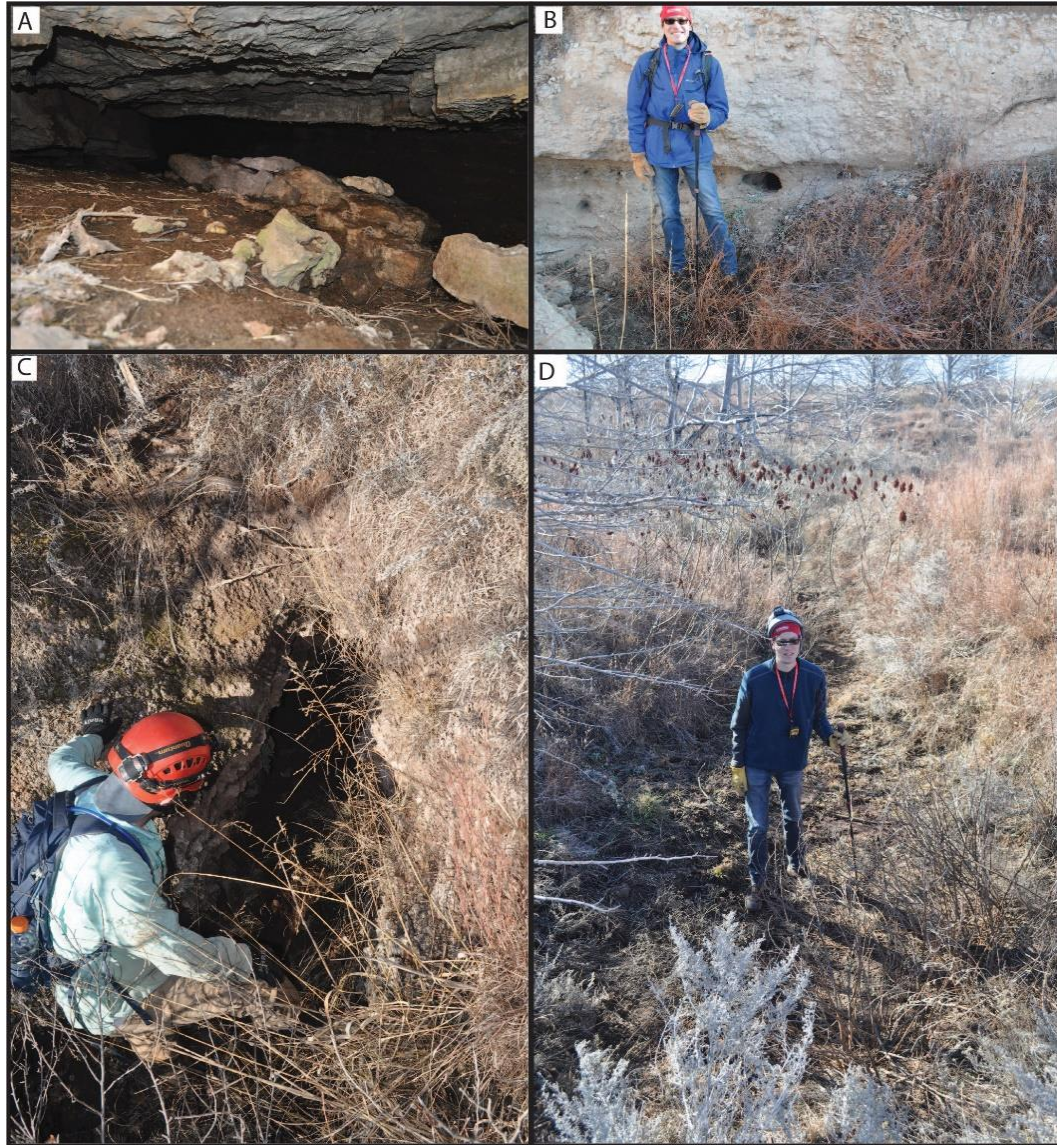
Figure 7. A variety of karst features present in Barber County such as A) caves, B) Epikarst, C) Swallow Holes and D) Sinkholes.

CHAPTER III

STATEMENT OF PROBLEM

3.1   Chapter Overview

Prior to outlining key literature to develop the background knowledge for understanding this research, the problems this research answers are presented in this chapter. During the initial stages of this research, a detailed search of the karst literature was preformed to identify a gap in the knowledge with the discipline and the region. Once gaps were identified, testable problems were developed to answer as the primary goals of this research.

3.2   Identification of a Gap in Research

Research that develops predictive models for karst features that are geographically specific has only come to light around 2010, and research within this discipline continues to evolve based on the increased accuracy of data and our changing planet (Doctor and Young, 2013, Yilmaz et al., 2011). There has not been a predictive model for karst features created for Barber County, Kansas. Other karst feature predictability models have been successfully deployed in other parts of the world such as Spain (Galve et al., 2009); however, most studies focus on the identification of surficial karst features using various geospatial data instead of prediction of karst features such as caves (Doctor and Young, 2013).

Petrologically, the Blaine Formation of Barber County, Kansas has been documented to contain a variety of strata (Benison et al., 2015); however, local scale variations have not been evaluated. The petrographic portion of this study will refine

local variations of the Blaine Formation to better understand the geologic controls on karst formation.

The problems addressed with the completion of this thesis are: 1) to predict karst features on a localized scale on a privately owned ranch within Barber County, Kansas and 2) determine the local nature of the geologic control on karst formation using petrology.

CHAPTER IV

LITERATURE REVIEW

4.1   Chapter Overview

This chapter outlines key concepts that are not specific to the region but are necessary for the background of this research. The literature review spans the basic understanding of karst, remote sensing platforms, GIS, and karst feature predictability in other regions of the world. Literature from this section will be used to put this research into perspective of previously conducted similar studies.

4.2   *Karst*

Karst is a landscape that develops on soluble rocks (White, 1988; Ford and Williams, 1989; Palmer, 2007). Karst topography contains features such as sinking streams, caves, sinkholes, and springs. Sinking streams disappear underneath the ground surface at a distinct area or sink point (Palmer, 2007). Sinking streams are concentrated input locations of water resulting in recharge of the karst aquifer (White, 1988; Ford and Williams, 1989). Cave are natural voids within the subsurface that are large enough to admit a human (Palmer, 2007). These karst features are formed by the dissolution of bedrock by infiltrating water (White, 1988; Ford and Williams, 1989; Palmer, 2007). Sinkholes (dolines) are depressions with an enclosed bowl shape usually found in karst terranes but may also form in non-karst terranes known as pseudokarst (White, 1988; Ford and Williams, 1989; Palmer, 2007). There are different classifications of sinkholes according to the process of formation. The types of sinkholes include: solution, collapse, dropout, buried, caprock, and suffusion (Waltham et al., 2005; Ford and Williams, 1989).

18

Sinkholes can range in depth from less than a meter to hundreds of meters and can also merge together to form compound sinkholes that have more than one infiltration point (White, 1988). Springs represent a zone where groundwater resurgence occurs at the land surface, provided an outlet for the karst aquifer (Ford and Williams, 1989).

Dissolution - Limestone Karst

Dissolution of carbonate rocks by carbonic acid is the dominant process that forms karst features within limestone bedrock. This process when meteoric water reacts with atmospheric carbon dioxide and further react with soil carbon dioxide creating carbonic acid (Waltham, 2005). Carbonic acid dissolves the bedrock creating karst features. The process of meteoric water derived carbonic acid dissolution on carbonate rocks takes longer than simple ionic dissolution because it depends on the amount of acid that controls the speed of the reaction (White, 1988). The chemical formula for limestone dissolution is below (Equation 1).

$$CaCO_3(Calcite) + H_2CO_3 \leftrightarrow Ca^{2+} + 2HCO_3^{2-} \qquad \text{(Equation 1)}$$
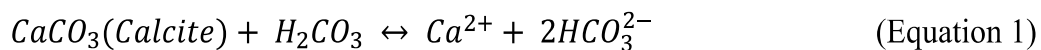
Dissolution - *Evaporite Karst*

Limestone is not the only soluble bedrock that develops significant karst landscapes. Evaporite bedrock dissolution occurs faster than carbonate dissolution due to the solubility differences (Raines and Dewers, 1997; Johnson, 1997). Most evaporite sequences are mixed with carbonates and evaporites. In these mixed sequences, significant karst features have been demonstrated to preferentially form in gypsum layers where the water is under-saturated with respect to gypsum (Palmer, 2007, Ford and

Williams, 1989, White, 1988, Yilmaz et al., 2011). Simple ionic dissolution of gypsum

demonstrates the principle method of evaporite dissolution (Equation 2).

$$CaSO_4 \cdot 2H_2O \ (gypsum) \ \leftrightarrow \ Ca^{2+}(aq) + SO_4^{2-}(aq) \qquad \text{(Equation 2)}$$
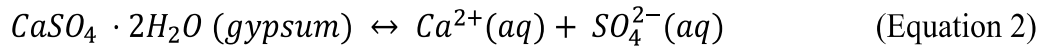
Gypsum ($CaSO_4 \bullet 2H_2O$) is a common evaporite mineral that dissolves rapidly by

ionic dissolution, producing karst features without the need for an acidic solution. The

solubility of subsurface gypsum is increased by subsurface pressure in the bedrock and

decreasing mineral grain size (Klimchouk, 1996). A more detailed description of gypsum

karst can be found in the following sources (Klimchouk, 1996; Benison et al., 2015;

Gauvey, 2019).

4.3   GIS and Remote Sensing Applied to Karst Landscapes

4.3.1   Field Mapping Karst Features

Field mapping karst features takes a longer amount of time than using previous

data collected from topographic maps (Hubbard, 2003). Morphometry, which is defined

as the measurement and analysis of the shape of earths landforms (Bates and Jackson,

1987), and is useful for grouping similar landforms together when mapping karst features

(Hyland, 2005; Ford and Williams, 1989). The use of Airborne Laser Swath Mapping

(ALSM) has been shown to not be a useful way to map karst features unless a large

amount of aerial photography was being used (Seale et al., 2008). Ground truthing

sometimes produces features that must be incorporated into data sets from field mapping

(Siart et al., 2009). Handheld (Global Positioning System) GPS unit are used in the field

for navigation to field locations, recording exact coordinates for new features, and begin

a preliminary analysis of the landscape features (Cornelius et al., 1994).

4.3.2   GIS analysis using ArcMap

Many different tools within the ArcMap software platform can be used in conjunction to create karst feature predictability models. The nearest neighbor distance tool is the most useful when creating predictability maps when the sinkholes are more clustered, and the density model is more useful when the sinkholes are dispersed across the land surface (Galve et al., 2009). An understanding of what controls sinkhole collapse is needed to better create predictability maps for the future, and the Normalized Difference Vegetation Index (NDVI) can assist with that understanding (Yilmaz, 2007). The creation of a karst feature predictability model in ArcMap is made considerably easier by combining multiple variables in karst feature prediction such as: the Digital Elevation Model (DEM), satellite imagery, elevation, slope, aspect, ground truthing in the field, and the distance to the drainage feature (Theilen-Willige et al., 2014; Ozdemir, 2016; and Kresic, 2013). One of the most common methods to predict karst features is using the Logistic Regression tool within ArcMap (Ozdemir, 2016).

Another method to separate sediment filled depressions from vegetation and bare rock would be to use the sink-fill tool (Siart et al., 2009). Using the Topographic Position Index (TPI) to calculate the elevation difference between a point on a DEM and the neighboring pixel is an emerging way to detect karst features (Doctor and Young, 2013). Reconditioning LiDAR using the watershed analysis tool within ArcMap is one method to detect karst features (Doctor and Young, 2013). Using the contour tool in ArcMap and looking for nested polygons, which are depression contour lines that are inside one another, represent complex depressions or more than one sinkhole when classifying karst features (Angel et al., 2004). If a complex depression had an innermost polygon, it would

21

be classified as a singular depression when creating karst feature predictability maps (Angel et al., 2004). Angel et al., 2004 constructed another classification for karst features that contained an innermost polygon that would be classified as a singular depression.

4.3.3   Remote Sensing Platforms

The organizations that use remote sensing technology have ranged from governmental agencies such as the National Aeronautics and Space Administration (NASA) to the private citizen (Siegal et al., 1980). Delineating features on the earth's surface is made considerably easier by the use of remote sensing. Light Detection and Ranging (LiDAR) is one type of remote sensing that uses lasers that reflect off the earth's surface from a platform mounted on either an aircraft or satellite to compute the elevation of the earth's surface.

Several remote sensing acquisition systems and software platforms were used in this thesis, which included: ASTER, LANDSAT, and Quickbird (acquisition systems) and MicroDEM, SAGA GIS, The ASTER (Advanced Spaceborne Thermal Emission and Reflection Radiometer) mission is a collaboration between the NASA Jet Propulsion Laboratory and Japan's Ministry of Economic Trade and Industry (METI) that started collecting data in the year 2000. The ASTER data is imagery of the earth's surface collected via satellite. The ASTER data can be acquisitioned from the USGS Earth Explorer online catalog as well as the NASA Earth Data catalog. LANDSAT (Land Remote Sensing Satellite System) is a satellite that takes images of earth continuously and has been doing so since the 1970s. This imagery can be downloaded from the USGS website or the NASA imagery portal. Quickbird is a satellite that is operated by the

company Digital Globe that collects imagery of the earth surface and was launched in 2001. This Quickbird imagery is available by purchase from Digital Globe, which is a subsidiary of the company MAXAR as of the year 2019.

CHAPTER V

METHODS OF INVESTIGATION

5.1   Chapter Overview

This chapter presents the methods to answer the problems previously identified. A

general summary is given before specific methods within GIS are discussed in detail.

Two predictive models were created and used in conjunction with other GIS functions to

create field validation points. These models were used to create a vulnerability map for

the probability of hazards associated with karst features on the property. Finally, standard

petrographic techniques are outlined for the analyses of the geologic composition of the

known karst forming layer on the property. These techniques are outlined with a large

number of figures for future reference for researchers using the equipment in the Rock

Lab of the Department of Geosciences at Fort Hays State University.

5.2   Summary of Approach to Creating the Predictive Models

These hypotheses were first tested by creating a predictive model using various

tools in the Environmental Systems Research Institute (ESRI) ArcMap software platform

version 10.7.1. Some of the geospatial layers used in operations included slope and

aspect, nearest neighbor elevation, NDVI, land cover/land use, distance to hydrologic

features, and detailed subsurface geology. Remote sensing was conducted using

hyperspectral imagery to determine stressed vegetation, which could assist in the viewing

of karst features and possible reconnaissance areas to study. The remote sensing analysis

was conducted at Fort Hays State University in the Geographic Information Systems

(GIS) Laboratory. This model was validated by doing ground-truthing fieldwork in

November 2019. This field work assessed the accuracy of predicting the locations of sinkholes and other karst features within the study area.

Two initial predictive models were created: the Non-Normalized and Normalized and Weighted with researcher optimization. The Non-Normalized model consisted of variables being entered into the raster calculator tool within ArcMap to create the model. The Normalized and Weighted with researcher optimization model consisted of different weights being placed on the variables before being placed into the raster calculator tool for model creation. These two models were combined into the final predictability model.

On the study location property, the geologic contact between the Permian Medicine Lodge Gypsum and the Flowerpot Shale appeared to be a control on the formation of karst features (Gauvey, 2019), and this contact may play an important role in predicting the location of unknown features due to the difference in solubility. Additionally, a dolomitic layer was documented within all karst features on this property (Gauvey, 2019). This dolomitic rock layer has a lower solubility compared to the overlying evaporite strata, contributing to the morphology and formation of these karst features. To examine the exact petrology of this dolomitic rock layer, rock samples were collected in order to document the lithology. These samples attempted to document the variability of this rock layer and determine if either a single dolomitic layer or multiple dolomitic layers were present. This research builds on previous work by Gauvey (2019) that documented the presence of the dolomitic layer(s) as a speleogenetic control on these karst features. When rock samples were collected, the locations and elevations were recorded using a handheld GPS unit. This GPS data helped determine the lateral

continuity of strata by comparing the relative elevation of samples with the lithology of samples.

5.3   GIS and Remote Sensing Methods

The first two goals of this thesis focused on the manipulation of spatial and remotely sensed data to predict the likelihood of the occurrence of a karst feature. Predictive models were field validated to determine accuracy. This model was combined with land cover/land use to create vulnerability maps. These vulnerability maps displayed the potential impact on human interactions with this karst landscape. Data used in this thesis originated from several public and proprietary sources.

5.3.1 Software Platforms

Multiple software platforms were used in this thesis, mainly ArcMap version 10.7.1 by ESRI. ArcMap aided in the map creation and data analysis for this research. Other software platforms included: MicroDEM, SAGA GIS and MNDNR (Minnesota Department of Natural Resources) GPS. MicroDEM, a freeware mapping program, was used to merge raster and vector datasets that were unable to be merged easily in ArcMap. SAGA GIS, an open source software, was used on personal computers unable to access the FHSU ArcMap license. MNDNRGPS, an open source software, was used to download the GPS data from a Garmin handheld GPS model eTrex® 10 to the computer for analysis and storage. The accuracy of the GPS unit is three meters. The software program ENVI 5.1 was used to analyze, classify, and display remotely sensed raster images.

5.3.2   Data Collection for GIS and Remote Sensing

First, data for Barber County, Kansas was collected or purchased when not open-source. The open-source data came from multiple online sources, such as: The Kansas Data Access Support Center (DASC), Kansas Geological Society (KGS), the United States Geological Survey (USGS), and the United States Department of Agriculture (USDA).

Data collected from DASC included: physical features (such as roads, surface hydrology, county shapefiles, and other physiographic features), and LiDAR. The DASC LiDAR data had a resolution of one meter and was collected in 2015, representing the most recent acquisition for Barber County, Kansas. The specific LiDAR type for analysis the model was the Bare Earth level of imagery. A (Digital Terrain Model) DTM was created from the LiDAR using ArcMap.

The dataset collected from the KGS was the geologic shapefile. Some of the KGS data (ex. local scale geologic maps) had to be digitized from non-georeferenced maps. Georeferenced topographic maps, ASTER scenes, and LANDSAT-8 scenes were obtained from the USGS. Land cover/land use datasets were collected from the USDA National Agriculture Statistics Service. All of these data were collected between May 2019 and December 2019.

Quickbird imagery was purchased from the company Digital Globe. This imagery was acquired in May 2018, had a resolution of 50 centimeters, and contained no cloud cover. The imagery was collected from the WorldView-3 spacecraft and was the only data purchased for this thesis.

GIS feature datasets were stored within a file geodatabase format. File geodatabases store up to one terabyte of data and allow for easy access within the ArcMap software platform. One feature dataset within the file geodatabase was created for each data layer used. This ensured that the data layers had the same geographic coordinate system within ArcMap. The specific coordinate system used for this geodatabase was North American Datum (NAD) 1983 Universal Transverse Mercator (UTM) Zone 14N. In some instances, the coordinate system that was used was identical to the above but the acronym HARN (High Accuracy Reference Network) was attached, which is an upgrade of NAD 1983 coordinates using GPS observations. This difference did not affect the reliability of the data within the geodatabase and the maps that resulted.

5.3.3   Initial Processing and Conditioning of Data

After data collection, multiple processing steps took place to condition data or create new layers for use in the predictive models. First, LiDAR DTM datasets were mosaicked together and clipped to the property extent. The Create Mosaic Dataset tool was used to create an empty mosaic dataset within the storage file geodatabase. After the empty mosaic dataset was created, the Add Raster's to Mosaic Dataset tool was used to add in the LiDAR sections to mosaic them together into one file. Multiple LiDAR datasets were needed to completely cover the property, but not all of these datasets combined extent was needed. Finally, the mosaicked LiDAR was clipped to the property boundary shapefile. From this mosaicked LiDAR coverage, DEMs and hillshade layers were created using the Spatial Analyst extension within ArcMap. Slope and aspect were also created using Spatial Analyst in ArcMap. The distance from roads and hydrologic features was produced using the Euclidean Distance tool within Spatial Analyst. Other

28

minor adjustments to the data included: clipping to the extent of the property boundary, digitizing various geologic features, and merging features from multiple shapefiles into more manageable data sources.

This LANDSAT data was used to calculate the Normalized Difference Vegetation Index (NDVI) using ArcMap. NDVI showed vegetation levels within the study area on a percentage scale from zero to one (one is the most vegetated, and zero has the least amount of vegetation). ENVI 5.1 was used to stack the LANDSAT-8 layers into one digital file, which makes for easier integration into the next operation. This combined file was used in ArcMap for the calculation of NDVI. NDVI was calculated by using the fourth and fifth bands of the LANDSAT-8 imagery. These bands show different views of the earth's surface than otherwise visible from the human's point of view of the infrared spectrum. The NDVI was calculated using the NDVI tool within the image analysis tool of ArcMap using the reflectance and sun angle. Reflectance is divided by sun angle to calculate the NDVI for each pixel in the scene. Next, the NDVI average was calculated from 28 NDVI files using raster calculator.

Quickbird imagery was used determine detailed land cover on the property at a localized scale and to assist in pinpointing karst features in the field validation stage.

As mentioned above, not all data were available in an acceptable digital format. For the geologic data, a significant amount of time was spent digitizing a shapefile from existing geologic maps of the region. The geologic map that was digitized for this research is the detailed surficial geology map of Barber County map number M-106 from the KGS. The digitization was accomplished by creating line features representing the geologic contacts between units and connecting them with the boundary area of study.

Polygons were then created with the feature to polygon tool within ArcMap. Subtypes were created for the different geologic units. The final geologic map for the property is shown in (Figure 8). The detailed geology for the property was an important layer that to be included in the creation of the models.
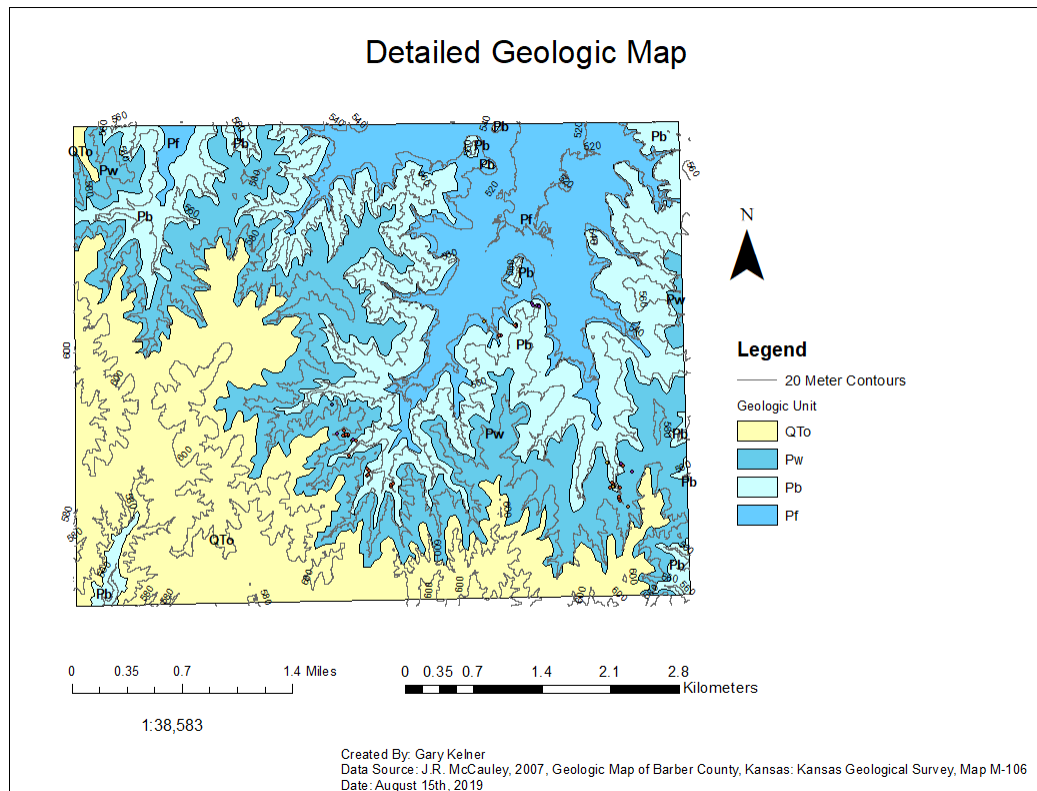
Figure 8. Detailed geologic map that was digitized of the property.

5.3.4   Model Creation using ArcMap: Model 1- Non-Normalization

This predictive model was created using the raster calculator tool function within the ArcMap Toolbox (Figure 9). This function allows the user to perform mathematical functions with layers in GIS such as addition and subtraction. This tool was being used to combine the different layers that make up the predictive model for karst features.
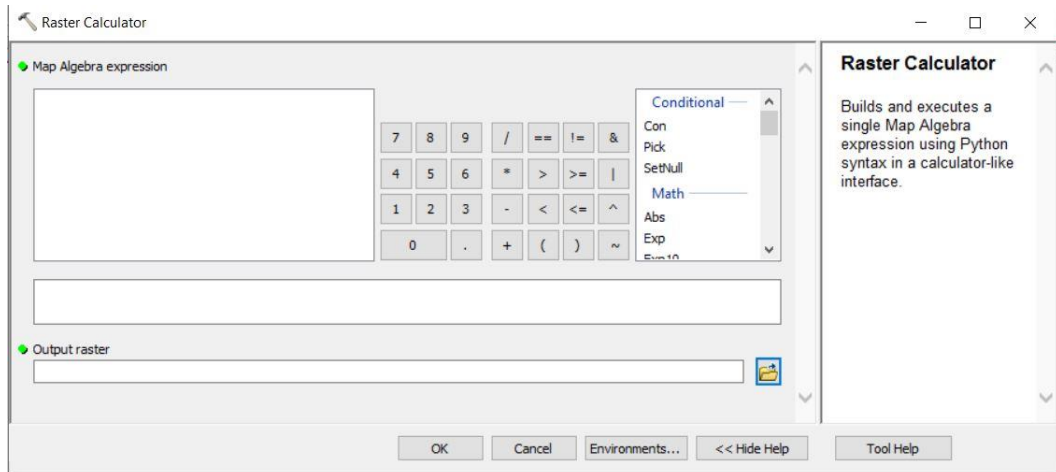
Figure 9: A screenshot of the Raster Calculator tool used within ArcGIS.

The model consisted of the geographic layers that were identified as being important in predicting karst features. This function would sum together all of the raster features that are necessary for karst feature prediction. The Conditional function was used because this categorizes the output of the variables being entered into the raster calculator. The output of this raster calculator tool would be the result of the karst feature prediction model. The output of the model was presented in a map for the reader. This map showed the amount of karst feature prediction from 0 to 100 or low to high karst feature predictability. This map was used as one part of a preliminary environmental assessment for the study area within Barber County, Kansas.

The first step to create the non-normalized model included creating Conditional Function #1, which involved elevations of known karst features. Conditional Function #1 calculated the elevation range of the karst features for the study area. This was done by using the following conditional function: (Equation 3).

Con(("DEM_Section">low elevation) & ("DEM_Section".
<High elevation)) , "DEM_Section") = outelevationrange_Section.   (Equation 3)

The output of this expression creates the elevation range from the lowest elevation to the highest elevation as shown by the DEM which is already in the GIS software.

The next step in the creation of the non-normalized modeled was writing Conditional Function #2, which incorporated land use data for karst features. Conditional Function #2 utilized the USDA land use data. The class of land use that was identified as important for karst feature formation was grass/pastureland. Conditional Function #2 was the following: (Equation 4)

Con("LandUse_USDA" , "outelevationrange_Section" ,
'' , "CLASS_NAME = 'Grass/Pasture' ") = outelevationLandUse_Section   (Equation 4)

This function calculated the intersection between elevation ranges of karst features and grass/pastureland cover. This intersection output would be used as the input for the next step of the model.

The next step of creating the non-normalized model was writing Conditional Function #3. This function calculated the intersection between the previous Conditional Function #2 and the distance from streams and farm roads. This calculation attempted to identify karst features associated with surface water and/or collapse. Conditional Function #3 was the following: (Equation 5)

Con((" farm roads_euclidean distance" < 4828.03) & ("hydrology_euclidean distance" <
4828.03) , " out elevationLandUse_Section") = outelevationdistance_section   (Equation 5)

These results identified the intersection between elevation, land use, the distance from roads as well, and the distance from surface water features for potential karst

features. The values above were miles converted to meters for use in the ArcMap system.

The next step of creating the non-normalized model was writing Conditional Function #4. This function identified the intersection of karst features within a specific aspect direction and slope with a certain degree with the previous Conditional Function #3 output. Conditional Function #4 was the following: (Equation 6)

Con((" DEM_Slope"<50) & (" outelevationdistance_section">0) ,
Con((" DEM_aspect">135) & ("DEM_aspect"<225) ,   (Equation 6)
"outelevationdistance_section" , 0)) = outraster_section

The results of this calculation showed the intersection of elevation, land use, distances from the roads and hydrologic features, and the aspect/slope of the landscape.

The final step of creating the non-normalized model was writing Conditional Function #5. Conditional Function #5 calculated the intersection of the previous outputs with the NDVI and local geology for karst features. Conditional Function #5 was the following: (Equation 7)

Con((" geology_units_raster">=geo unit raster number) & (geology
_units_raster">= geo unit raster number) , Con(("ndvi_month_section">1)   (Equation 7)
 & ("ndvi_month_section"<400) , "outraster_section" , 0))

Equations 4 through 7 had to be executed again after this initial run with the land use class changed in Equation 2 to deciduous forest because this model can only accommodate one land use class at a time within the raster calculator tool.

Another version of the model was created but instead of the weights being solely on the elevation of the data, the second version of the model was more focused on the

geology of the area. This model focused more on the geology due to the notion that karst features only form within specific geologic units that can be disseminated from the geologic map of the area.

5.3.5   Remote Sensing – Model 2- Normalized and Weighted with Researcher Optimization

The remote sensing was conducted using the Harris Geospatial software platform ENVI version 5.1 (32-bit) that is in the GIS laboratory at Fort Hays State University. This software was first used to perform the Sabin's ratio that used the ASTER data from 2007 that was collected from the USGS Earth Explorer online catalog as well as the NASA Earth Data online catalog. The data from 2007 was used because there was an incident in 2008 where a sensor stopped responding due to excessive heat, which concluded that all ASTER data post 2008 was unusable and does not have the imagery bands required for the analysis to be performed.

The additional variables used in the Normalized and Weighted Model were distance to the geologic contact between the Blaine and Flowerpot Formations, and ASTER Geology calculations (Sabin's Ratio). The distance to the geologic contact was calculated using nested buffers around a digitized contact vector file within ArcMap. The buffers closest to the geologic contact were given values of 10, and lower values were given as the distance from the contact increased. This is following the hypothesis that the geologic contact plays an important role in speleogenesis within Barber County (Gauvey, 2019). These nested buffers were converted from vector files to raster files to be utilized in raster calculator.

Sabin's Ratio was calculated using the Harris Geospatial software platform ENVI (Environment for Visualizing Images) version 5.1 (32-bit). ASTER data from 2007 was acquired and band ratios were used to calculate Sabin's Ratio. There were certain band ratios that were developed to show mineral occurrences on the land surface according to (Ourhzif et al., 2019). Sabin's ratio uses combinations of bands within the ASTER data and the equation is the following: (Band 4/Band 2, Band 6/Band 7, Band 10). The ratios were created using the band ratio tool within the ENVI toolbar and once the ratios were created, the band math tool was used to add together the resulting ratios to create the final output map. This Sabin's ratio shows the mineral composition of the study area. The following ratio: [(Band 6+Band 9/Band 7+Band 8), (Band 5+Band7/Band6), Band 2/Band 1] created a Red-Green-Blue (RGB) false color image of the ASTER data as the output. The initial false color raster image was reclassified based on having three known geologic materials at the surface (red shale, gypsum/gypsiferous soil, and sandstone). This reclassified output showed the potential gypsum deposits along with other similar units such as the gypsiferous soil that is commonly seen in the study area.

Similar to the non-normalized model, this model used the raster calculator tool function within the ArcMap Spatial Analyst Toolbox. Prior to inputting these raster files into the raster calculator, these files were normalized for the highest potential of karst feature prediction. This was accomplished by using previously identified karst features (74 karst features identified by Gauvey, 2019) to determine the range in values of every variable input into the model for this select set of training data. To determine the range in values for each variable, a 10-meter buffer was created around each known karst feature, and zonal statistics were calculated using ArcMap. This idealized range of each variable

allowed for the reclassification of the raster data into normalized datasets with a value of 10 assigned to the range of values associated with the training data (known karst features). Lower values were given to the reclassified data for values outside of the training data. This zonal statistical method using training data was performed on all of the variables input into this model.

Next, normalized variables were evenly weighted to create an initial model; however, this evenly weighted initial model did not perform as expected. This was determined by using a preliminary validation dataset (containing 15 additional karst features located by the authors) collected after Gauvey (2019) completed her work.

Finally, several efforts were attempted to manually optimize feature prediction using various weightings of variables. This was accomplished by varying the weights of variables until the preliminary validation dataset was adequately predicted. The optimized weights were determined to be 34.5% geologic contact, 27.6% ASTER Sabin's Ratio geology, 17.2% elevation, 10.3% Aspect, 6.9% slope, and 3.5% NDVI. When these weights were applied in raster calculator, the output file was scaled from 1-to-10 with higher values associated with higher predictions for the presence of karst features.

5.3.6   Comparison of the two models

Scaling of the model was completed using the raster calculator function within ArcMap. This was completed by multiplying the original model raster by the highest value of the model created using remote sensed data. This created a model that shows where the two models show similar data as well as where the models show differing data. This was useful because this showed areas to visit to ground truth the two models and see

if either was effective in predicting karst features within the study area. The output of this scaling showed two zones, either where one model thought that there was a karst feature or where both models thought there could be karst features.

5.3.7   Field Validation of the Predictive Models

The field validation was conducted during the weekend of November 23rd, 2019 and November 24th, 2019. Before the validation weekend, 50 points were chosen to visit based intersections of the output of the two models with sink-fill features (Figure 10).
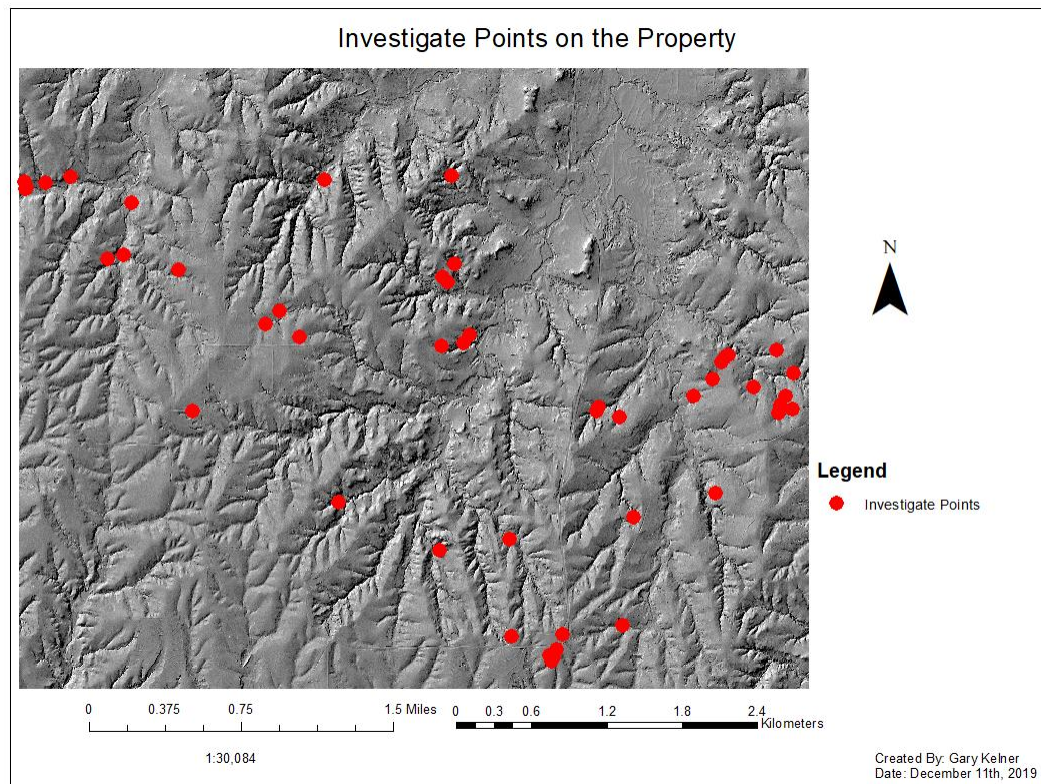
Figure 10. The investigate points chosen on the property.

The map was converted into a GeoTIFF file type that allows the map to be georeferenced on a mobile platform. A mobile application was used called Avenza Maps® on multiple handheld devices and tablets during the field verification weekend to

aid in the location of the points of interest and to guide the researchers to the point in question. If there was a karst feature present at the point, a pin was placed on the map within the app, and detailed notes were taken as well as the GPS coordinates of that location for further analysis.

5.3.8 Vulnerability Map

A map that predicted the vulnerability of infrastructure to karst hazards was created. This vulnerability map was created using the Normalized and Weighted Model. This model was used because of holes created by the distance to road function used in the Non-Normalized Model. First, a new field (float) was added into the attribute table of the land use raster file from the USDA. Each land use classification was assigned values of either one, five or ten (low, medium, or high, respectively) for the hazard level to infrastructure. Agriculture and woodlands were given low vulnerability values. Agriculture was given moderate vulnerability values. Roads and development were given high vulnerability values. The Lookup function was then used within the raster calculator to use the newly created vulnerability field in the calculation (Equation 8).

"Norm_Mod"*Lookup("Landuse_vulnerability","Vulnerability")   (Equation 8)

5.4 Petrographic Methods

Petrographic thin sections were created in order to examine the geologic composition of dolomitic layers found in association with various karst features. Standard petrographic thin sections were created by first using a water-cooled diamond saw (Figure 11) to trim bulk samples to a size of 1.5'' long by 1'' wide by ½'' thick (Figure 12).

Figure 11. Water-cooled diamond blade trim saw used to cut bulk samples to appropriate size for thin section creation.
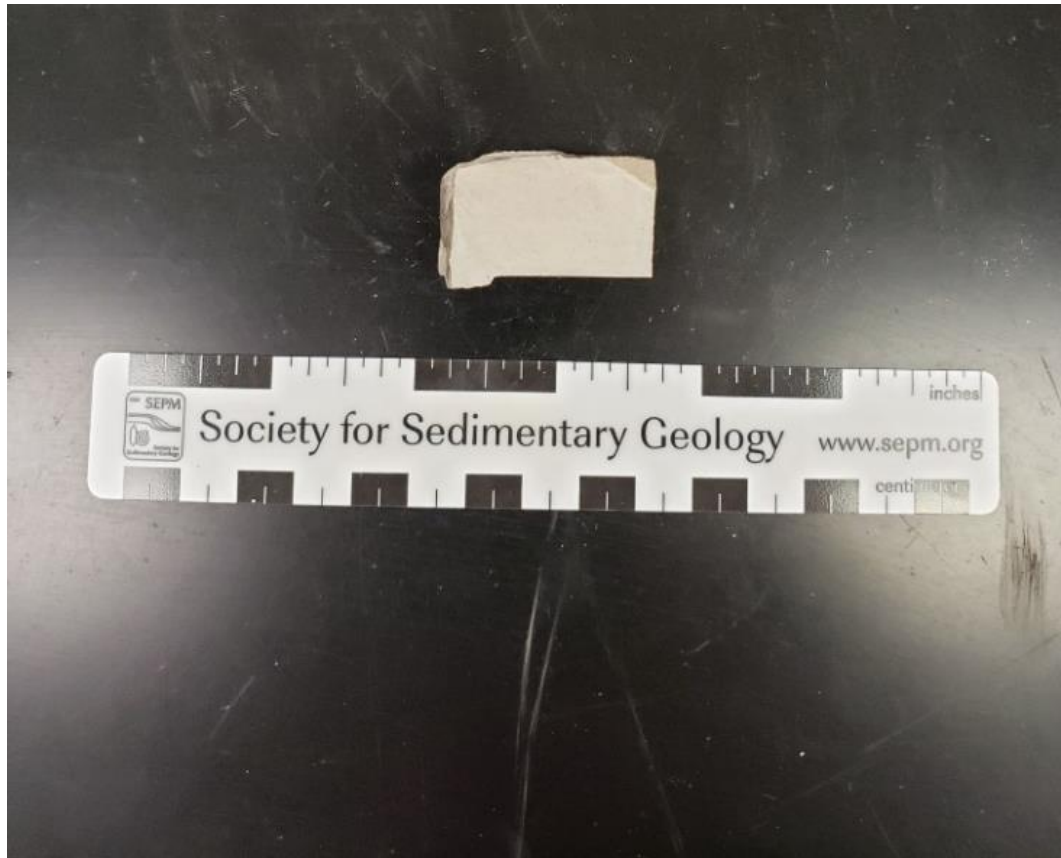
Figure 12. An example of a trimmed billet ready for attachment to glass microscope slide.

Trimmed samples (now referred to as billets) were ground on one side of the sample to remove saw chatter marks (uneven surfaces) and provide a relatively flat surface for adhering to a microscope slide. Optical ultraviolet adhesive (Norland Optical Adhesive NOA61) used to bond the trimmed rock samples to 1" by 2" glass microscope slides that were also ground on one side to facilitate adhesion of the optical adhesive. Samples were allowed to cure for 24 hours under an ultraviolet light-source until the adhesive was solid. Once the adhesive fully cured, excess rock was trimmed using a cutoff saw with vacuum sample holder. This produced a thinner slice of rock attached to a microscope; however, this slice of rock was still too thick for optical transmission using

a light microscope. Removal of excess rock material was accomplished using a

petrographic thin section grinding lap wheel (Figure 13).
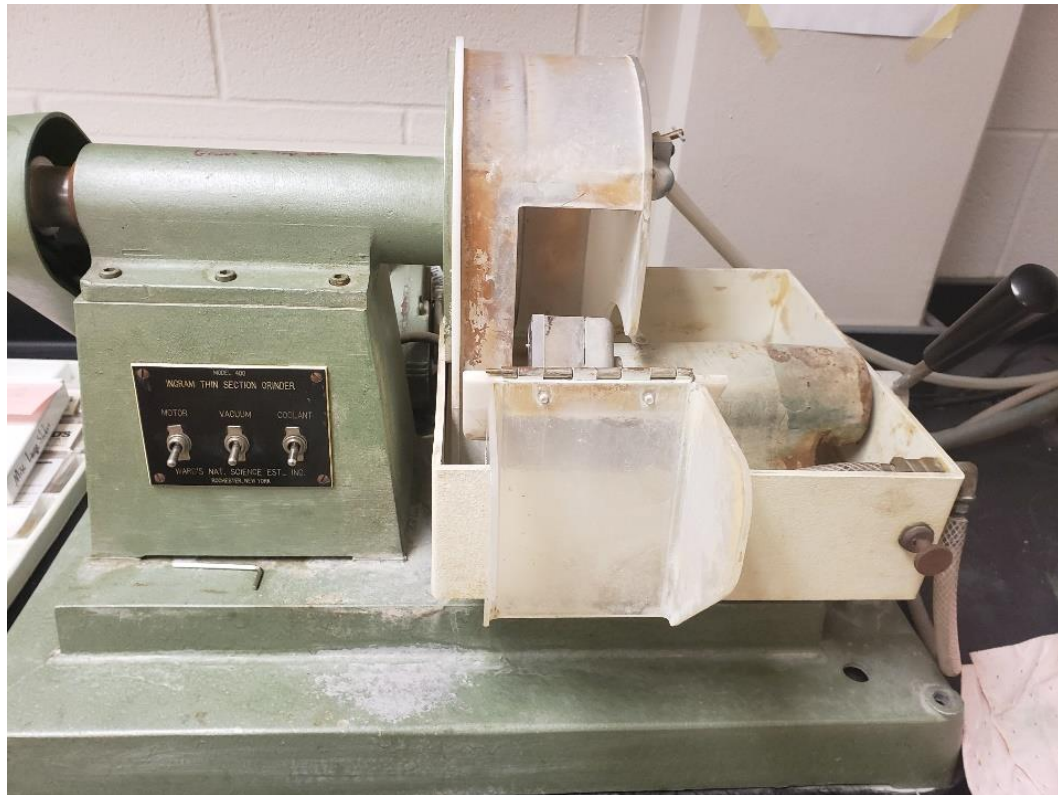
Figure 13. The Wards Thin Section Grinder which grinds off microns of rock to get to the optimal thickness of 30 microns.

Finishing of thin sections to a final thickness of 30 microns was accomplished by

step-wise hand grinding using silicon carbide grits of finer sizes for each step (320-grit,

600-grit, and 1000-grit) on a glass plate (Figure 14).

Figure 14. Hand grinding a thin section using different grades of silicon carbide grit, water and a glass plate.

The analyses of the petrographic thin sections were conducted using a Leica DM-EP Polarizing Light Microscope with an attached imaging system model Leica EC 3. The Leica-EZ imagery software suite was used for image acquisition and editing. Petrographic point counts were conducted by systematically moving the mechanical stage on the microscope to acquire 100-points to be identified and recording what was underneath the crosshairs of the petrographic microscope. A graduated stage and Lab Count Denominator were used to assist in the point count analysis (Figures 15 & 16). The results that were tabulated on the Lab Count Denominator were then entered into a Microsoft Excel Workbook for storage and later analysis.

Figure 15. The graduated stage that was used during the point count analysis of the petrographic thin sections.

Figure 16. The Lab Count Denominator that was used to count the various amounts of minerals when performing the point count.

After point counts were conducted, the thin sections were stained to differentiate dolomite and calcite cement using Alizarin Red-S (Hutchison, 1974). The staining process began by pouring 15 mL (milliliters) of Alizarin Red-S solution into small beakers. One half of one thin section was placed into the solution for one minute and then the excess stain was rinsed off as in (Figure 17). This was then repeated with the remaining thin sections.
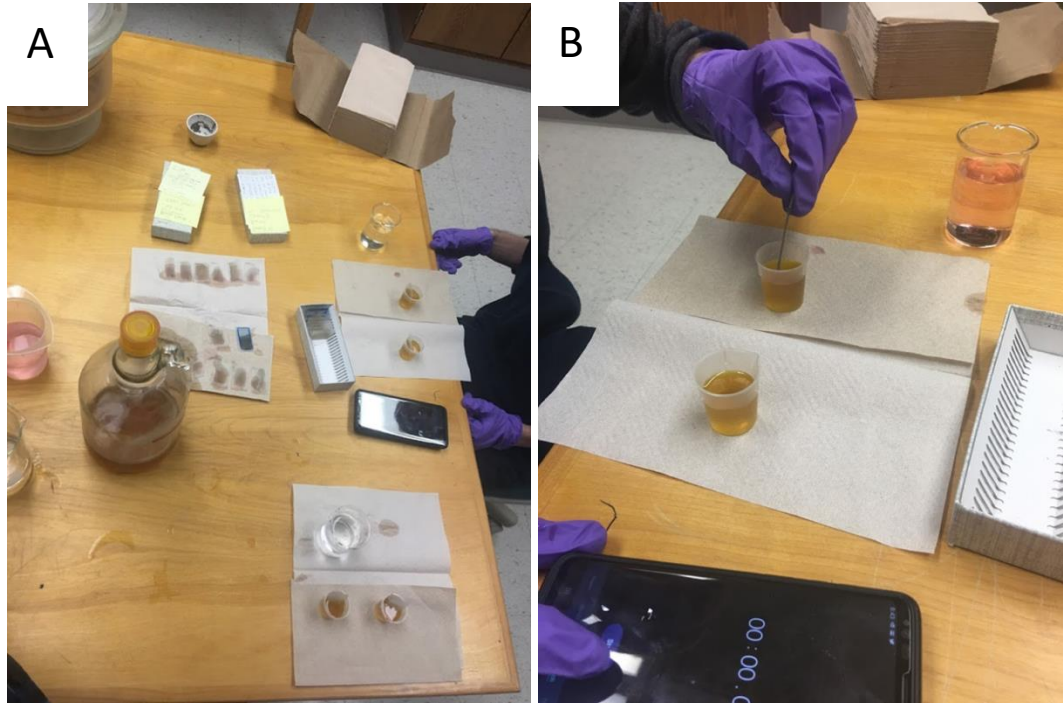
Figure 17. The thin sections were stained using Alizarin Red (A) and then the excess was rinsed off (B). One half of the thin section was submerged in the Alizarin Red for one minute.

CHAPTER VI

RESULTS & DISCUSSION

6.1   Chapter Overview

Due to the difficulty in separating results and interpretations when presenting GIS results, these sections were combined for this chapter. First, the karst feature predictability models and products are presented and discussed. The output layers used in each karst feature predictability model are presented below. The karst feature predictability models were moderately successful in the detection of karst features that were not visible from aerial imagery. Finally, the petrographic results are presented and discussed, especially focusing on their distribution and contribution to karst formation.

6.2   GIS and Remote Sensing

The various outputs to create the predictive models by GIS and Remote Sensing are shown below and discussed in brief detail in regard to the development of the predictive model. These outputs include: Hillshade, Slope, Aspect, and Distance from roads and hydrologic features, NDVI, Geologic maps (low and high resolution, Geologic contact, Land cover/land use, and Sink-fill. Previously identified karst features from Gauvey (2019) (Figure 18), were used to calculate zonal statistics for an area (10-meter buffer) around karst features to determine parameters for model inputs. The 'Zonal Statistics as a Table' tool was used in ArcMap to calculate the mean, median and mode values for the various outputs listed above.

Figure 18. Identifying karst features utilized in the calculation of zonal statistics.

The Hillshade is derived from the LiDAR DTM (Figure 19). The Hillshade for the study area shows the relief, and the LiDAR DTM contains the elevation ranges for the study area. The elevation ranges of the area ranged from 500 to 700 meters ± one meter based on the LiDAR DTM data. Based on zonal statistics for karst features, karst features are found at an average elevation of 564.64 (range of 540.8 – 590.73). The hillshade will be used later for calculating the sink-fill by using the sink-fill function within ArcMap.
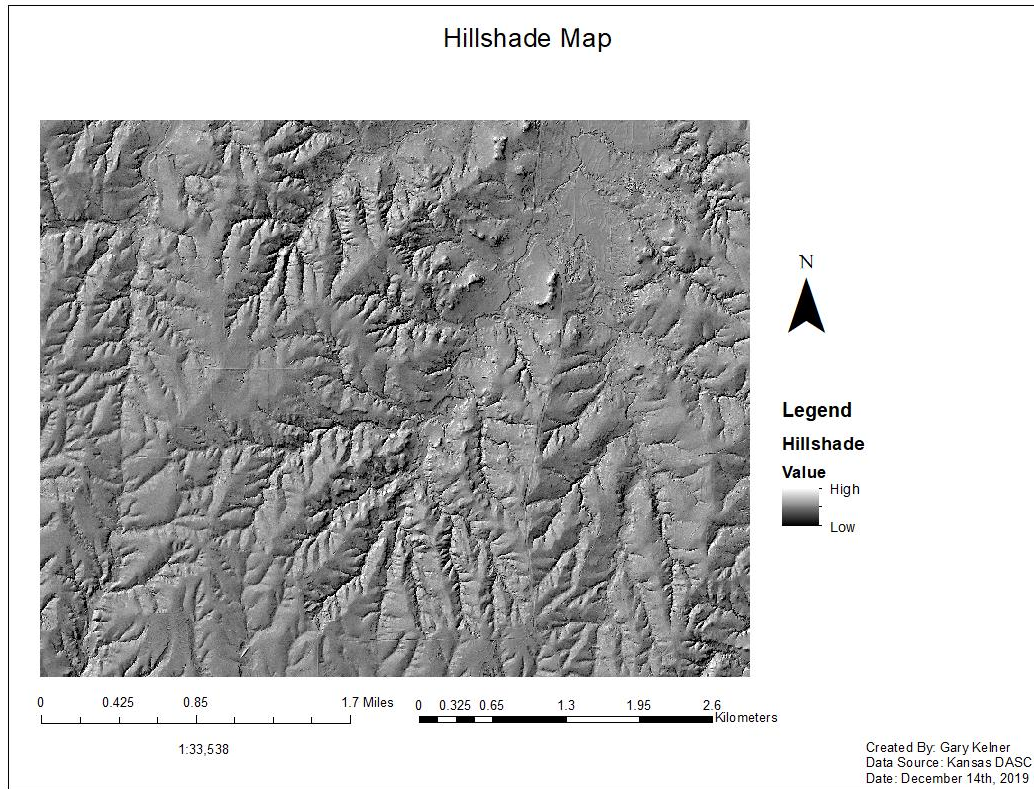
Figure 19. Study area Hillshade Map ('Red Hills' Topology).

Slope is a measure of the gradient of the land surface in degrees. Slope is calculated from the LiDAR DTM using the slope function in ArcMap (Figure 20). The overall range in slope is from zero to 76.3 degrees. Slope was used in the creation of the prediction model to assist in the prediction of karst features. It is believed that lower slope values represent landscapes more prone to karst feature collapse than higher slope areas based on field observations. The average slope around karst features was (6.0 – 20.41).
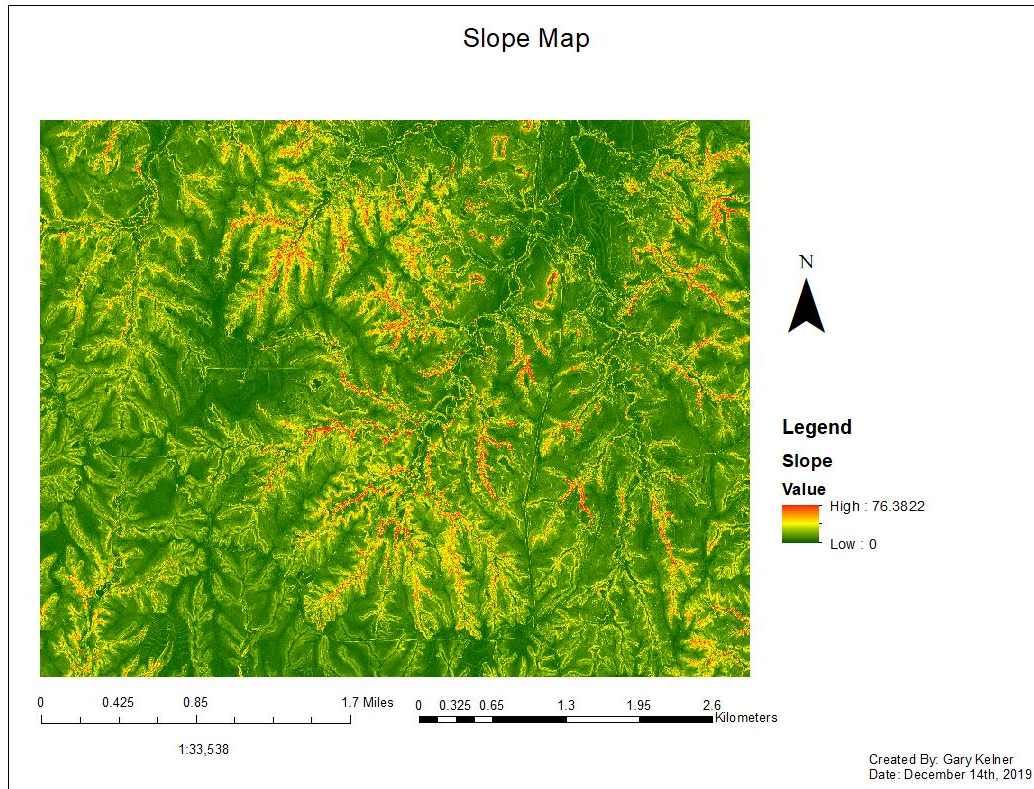
Figure 20. Study Area slope map in degrees.

Aspect is a measure of the direction that a slope faces. Aspect is calculated from the slope using the aspect tool in ArcMap. Aspect is generally displayed by compass direction (Figure 21). Based on the zonal statistics for karst features, the average aspect direction was approximately south (171°). Southern facing slopes receive more direct sunlight throughout the year in the northern hemisphere. This increase in direct sunlight received should affect the amount of water available and vegetation, which both may influence karst development and/or expression.
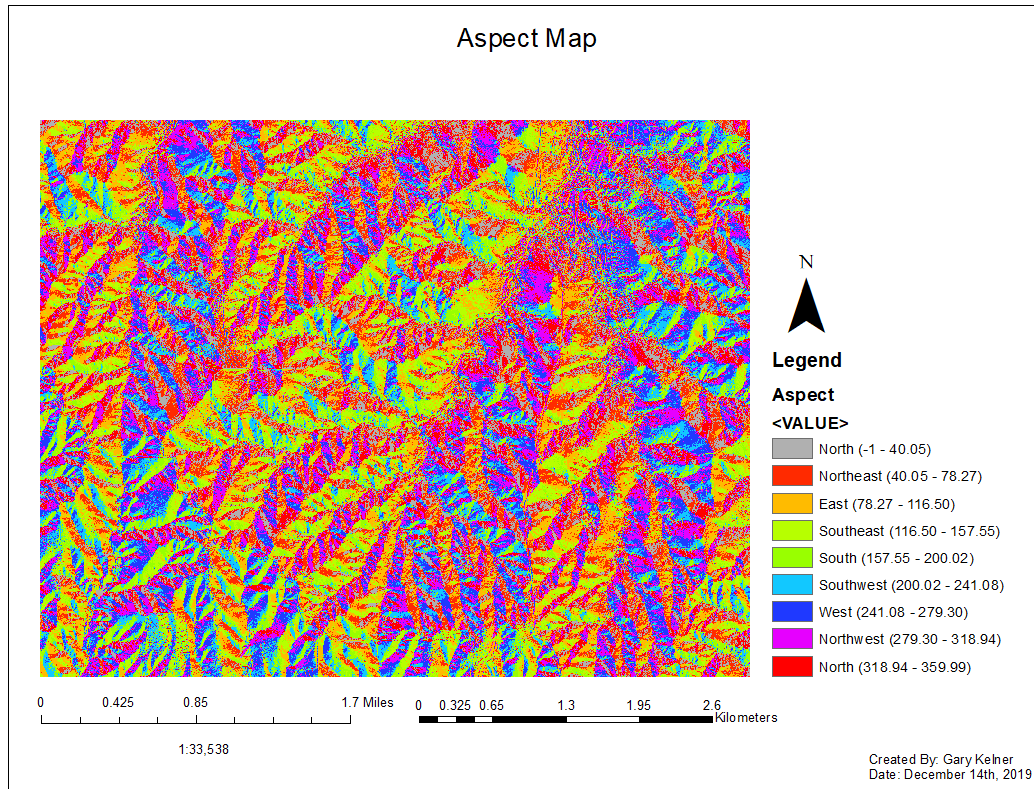
Figure 21. Study Area aspect map.

The distance from roads and hydrologic features is calculated using the Euclidian distance tool in ArcMap (Figures 22 & 23). The distance from hydrologic features is larger than the distance from roads because there are fewer hydrologic features in this area of Barber County compared to roads. The farthest distance from a road is 1543 meters, and the farthest distance from a hydrologic feature is 4777 meters. The western portion of the property is farthest from the major hydrologic features. Roads provide a relatively impervious surface that promotes surface water runoff. This suggests that roads may contribute to localized karst development, and this relationship attenuates away from these impervious surfaces. Surface hydrologic features provide infiltration sources for standing water, which should increase the likelihood of surface karst development. Moving away from hydrologic features should decrease this likelihood.

50
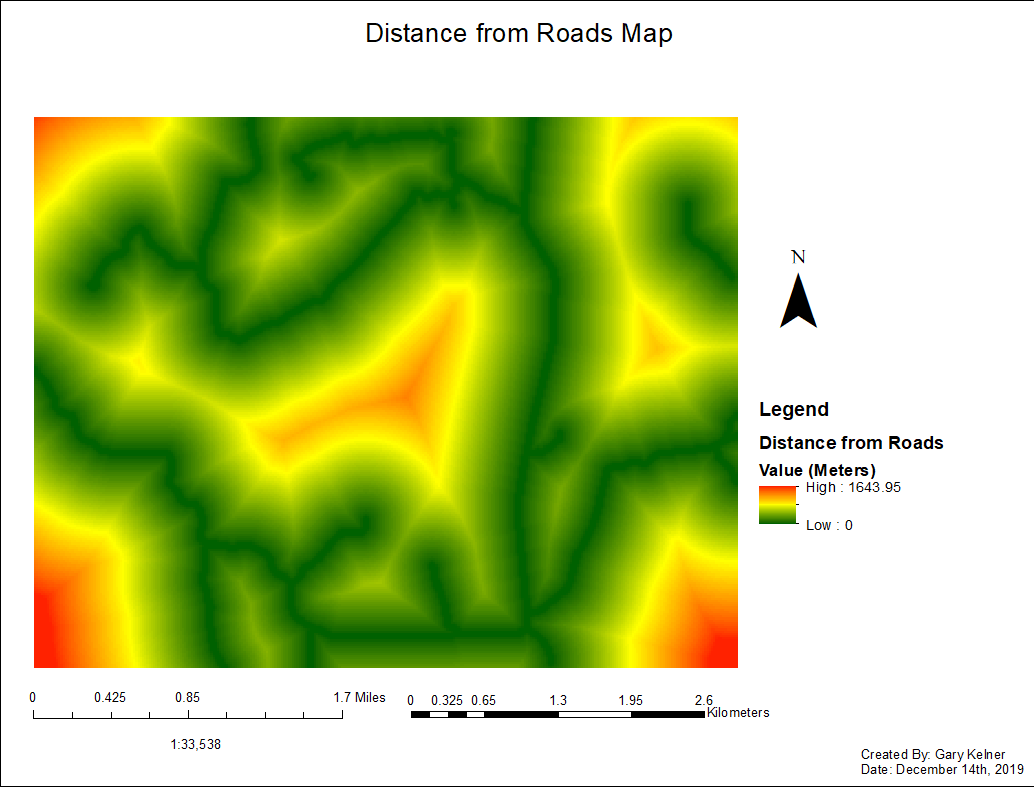
Figure 22. Study Area distance from roads map.
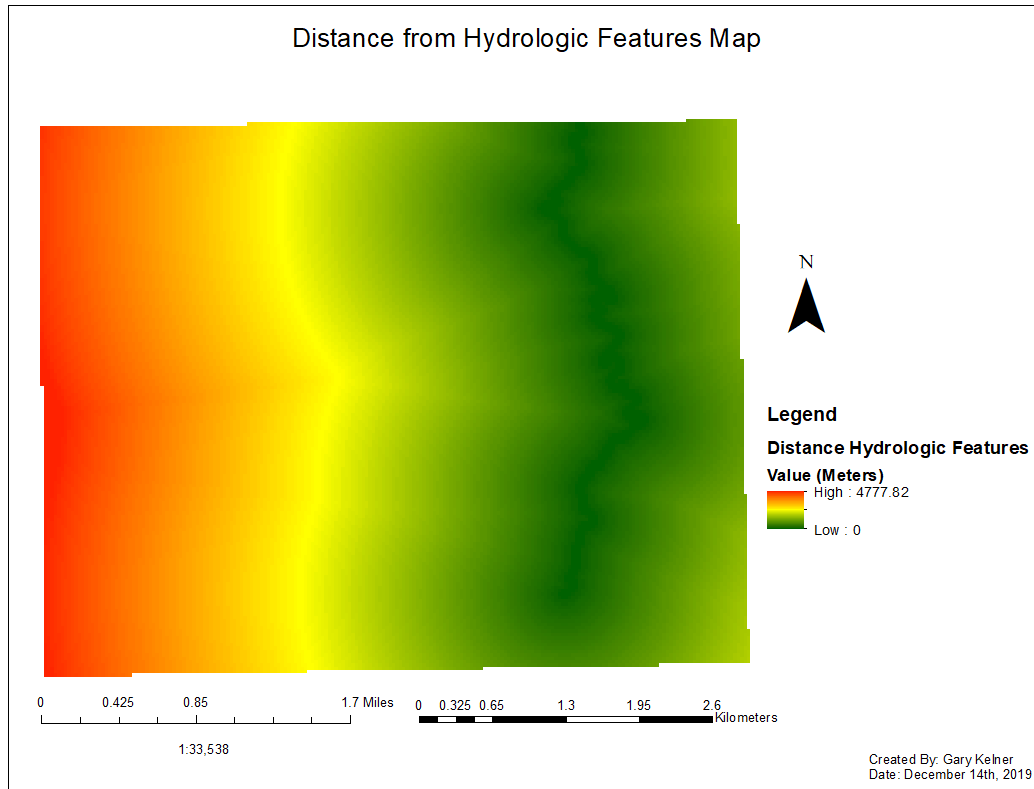
Figure 23. Study Area distance from hydrologic features map.

NDVI for the study area was calculated from the following months: March, April, May, August, September, November, and December from the year 2018. NDVI maps for each month can be found in Appendix H. The NDVI Average was calculated from those seven months using Raster Calculator (Figure 24). This NDVI Average layer was used in each of the predictive models. The average NDVI value for the property ranged from -1 to 1, while the average value for areas around karst features ranged from 0.0149 to 0.0219. Locations near karst features should have a higher NDVI than areas farther away from karst features. The range in NDVI around karst features suggests that these areas show little changes in the vegetation based on climatic differences (ex. drought or flooding).
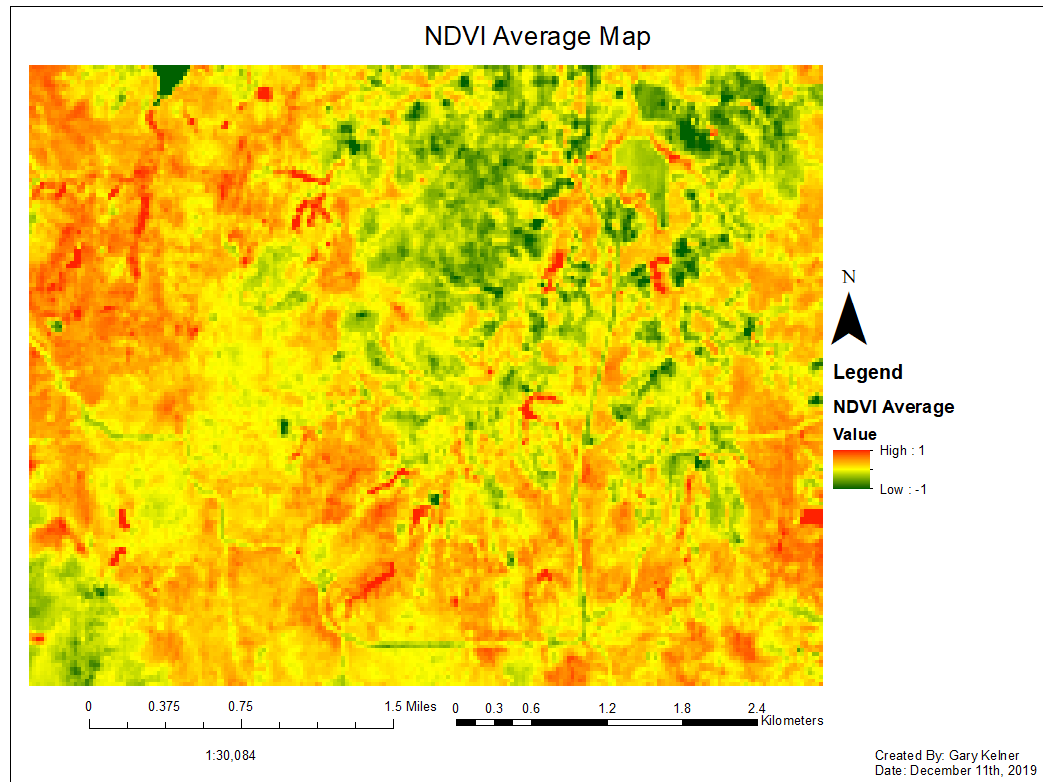
Figure 24. Study Area NDVI average map.

      The land cover/land use for the area of study consisted of mostly rangeland and agriculture (Figure 25). There were minor occurrences of developed, vegetated, and woodland land cover on the property. The non-normalized model utilized land cover/land use, and this layer also was used in created the vulnerability map.
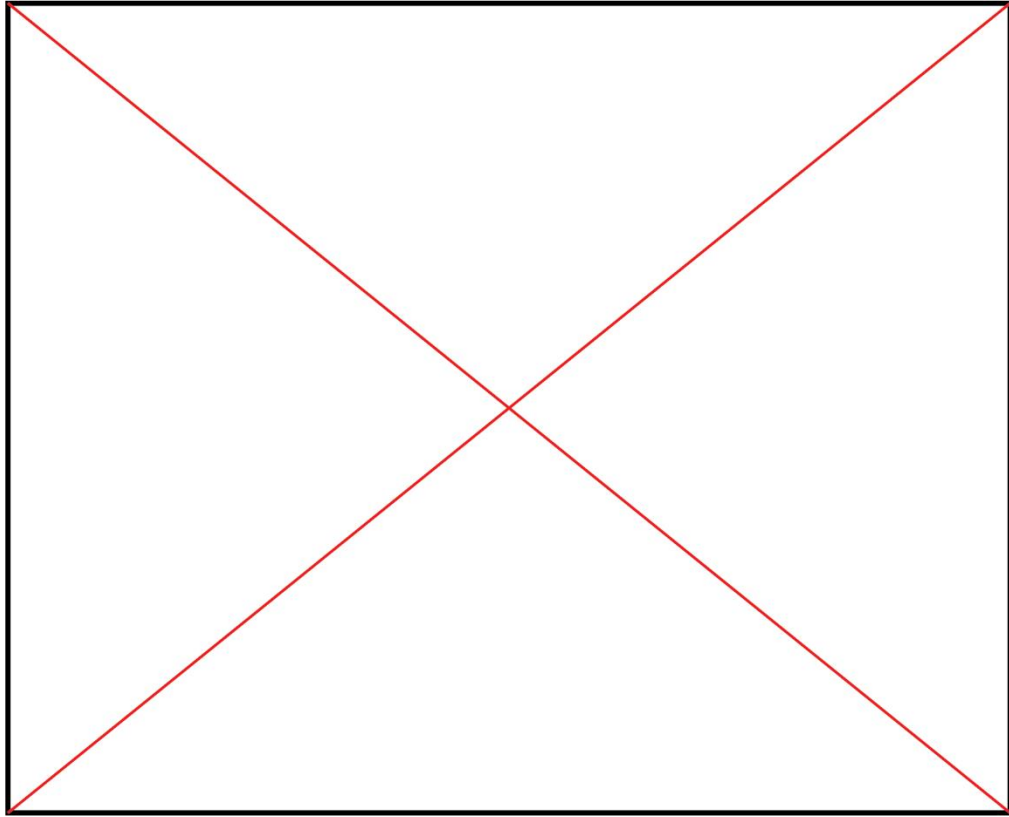
Figure 25. Study Area Land Cover / Land Use map.

  The sink-fill function shows all of the hydrologically enclosed depressions that are in the area of study (Figure 26). These depressions represent a combination of karst depressions (sinkholes) and non-karst features (cattle ponds). A large amount of these depressions appeared to be cattle ponds based on field and imagery observations. Due to time constraints, the large number (806), and the difficulty of differentiating them, the predictive models narrowed down these features for field validation by selecting sink-fill features that intersect the karst agreement model.
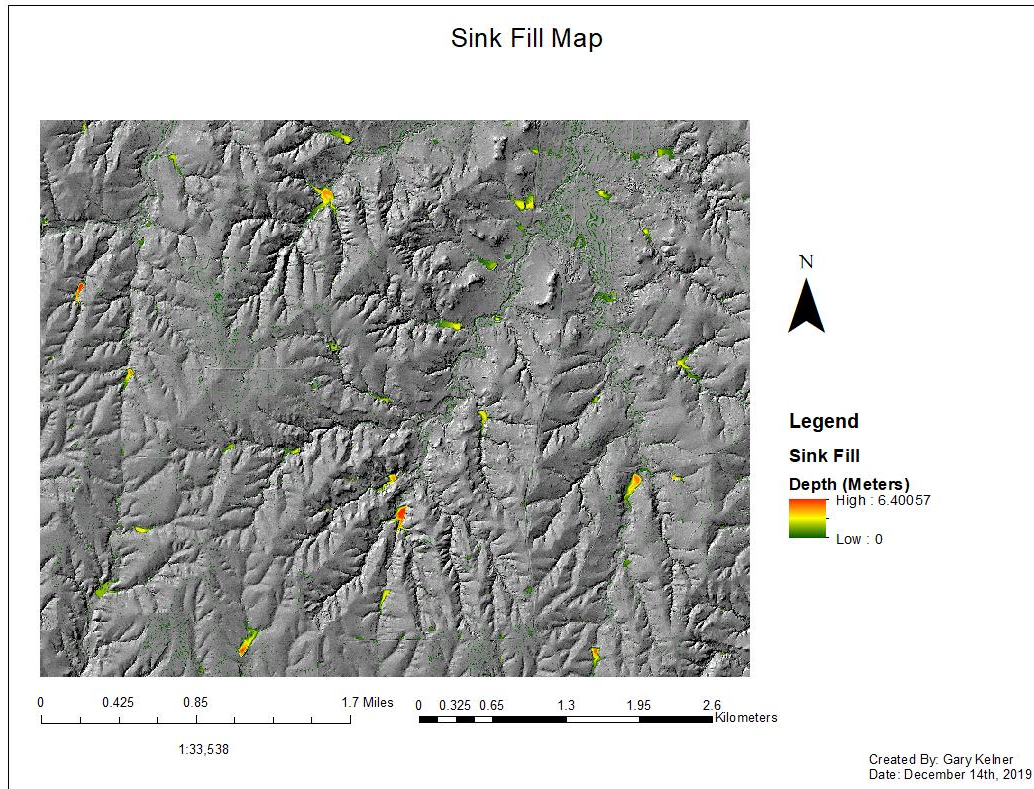
Figure 26. The result of the sink fill function within ArcMap for the study area.

The general geology of the Barber County, Kansas was too poor in resolution for any meaningful analysis at the local scale to determine karst features (Figure 27). Instead, the detailed geology was digitized using ArcMap because the KGS did not have that layer readily available in digital format for this thesis. The original detailed geologic map from KGS was developed from aerial photograph interpretations and interpolated from key outcrops in the area (Figure 28). The contact between the Flowerpot Formation and the Blaine Formation was digitized from the detailed geologic map. Several errors were initially discovered that did not agree with field observations on the property. These errors were corrected in ArcMap when encountered (Figure 29); however, a significant portion of the property (specifically the northwest portion) remains unverified for

geologic accuracy. This new contact was also compared with digital imagery from

Digital Globe.
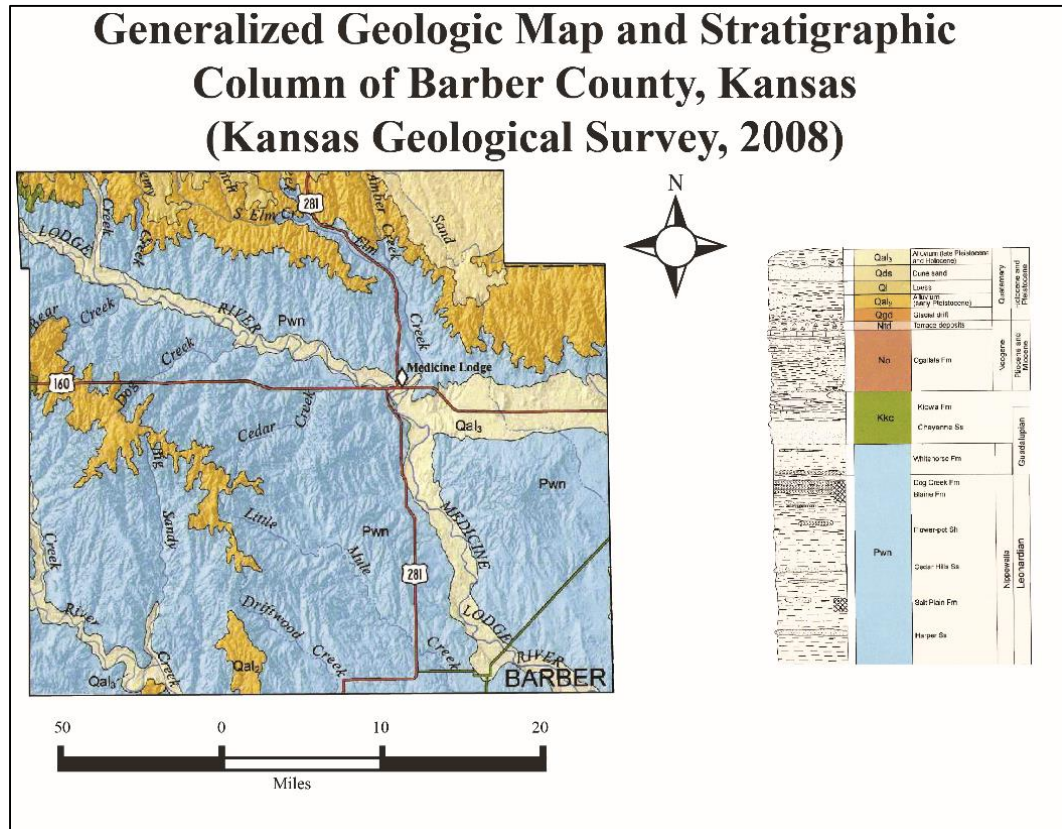
Figure 27. The generalized low resolution geologic map of Barber County, Kansas.
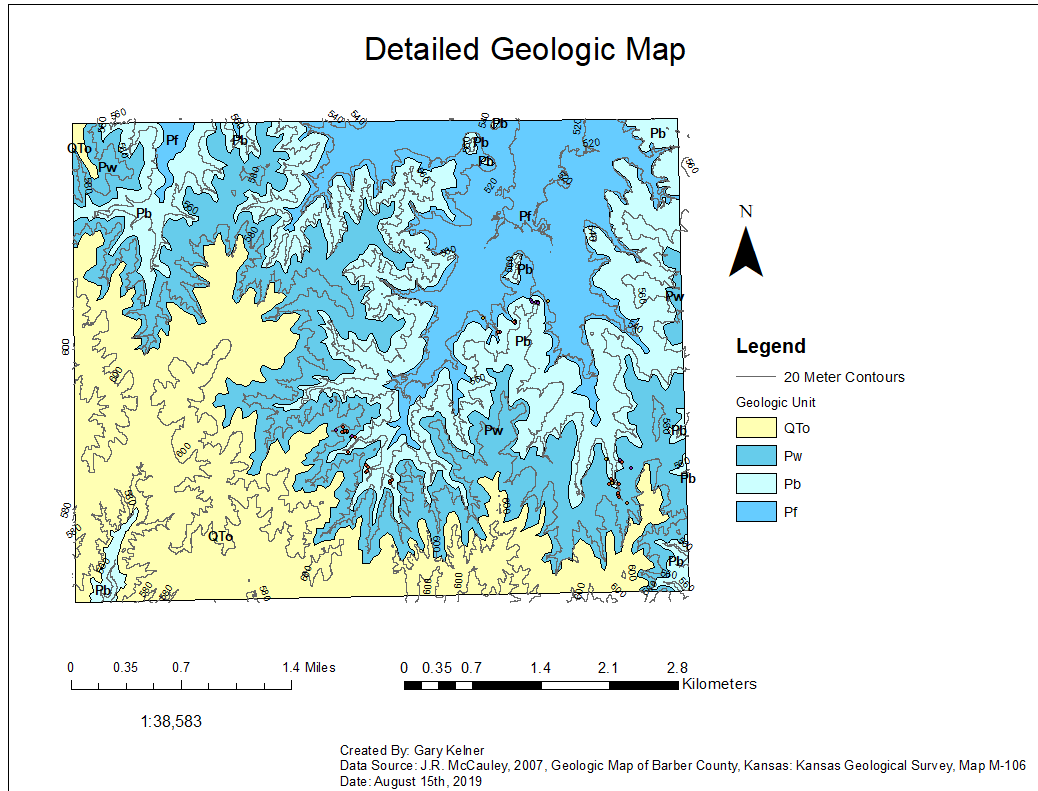
Figure 28. The detailed geologic map of the property within Barber County, Kansas.
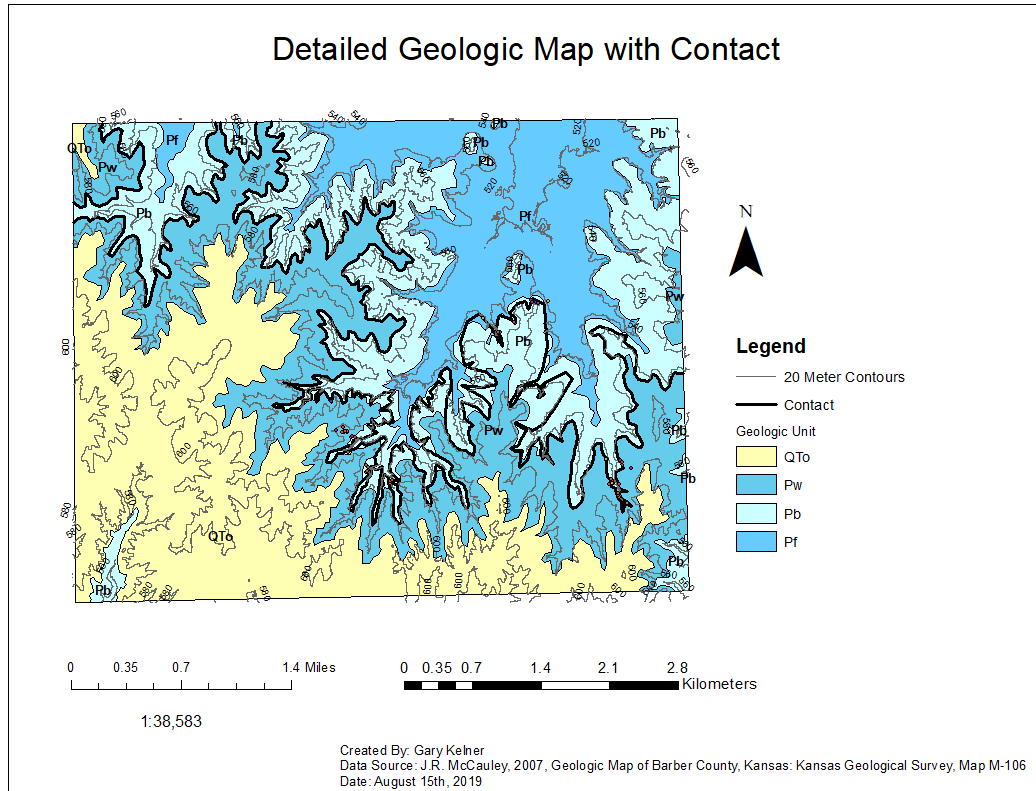
Figure 29. The geologic map showing the contact between the Flowerpot Formation and the Blaine Formation.

6.3   Model 1: Non-normalized Model Output

The non-normalized model utilized various landscape parameters to predict karst feature location (Figure 30). Areas are displayed as a high probability (red and yellow) to low probability (greens) for karst feature development (Figure 30). Generally, this model predicts high karst probability in the southwestern to western portion of the property, especially near topographic highs and areas of low slope. Blank areas represent errors produced by using the Euclidean Distance function.
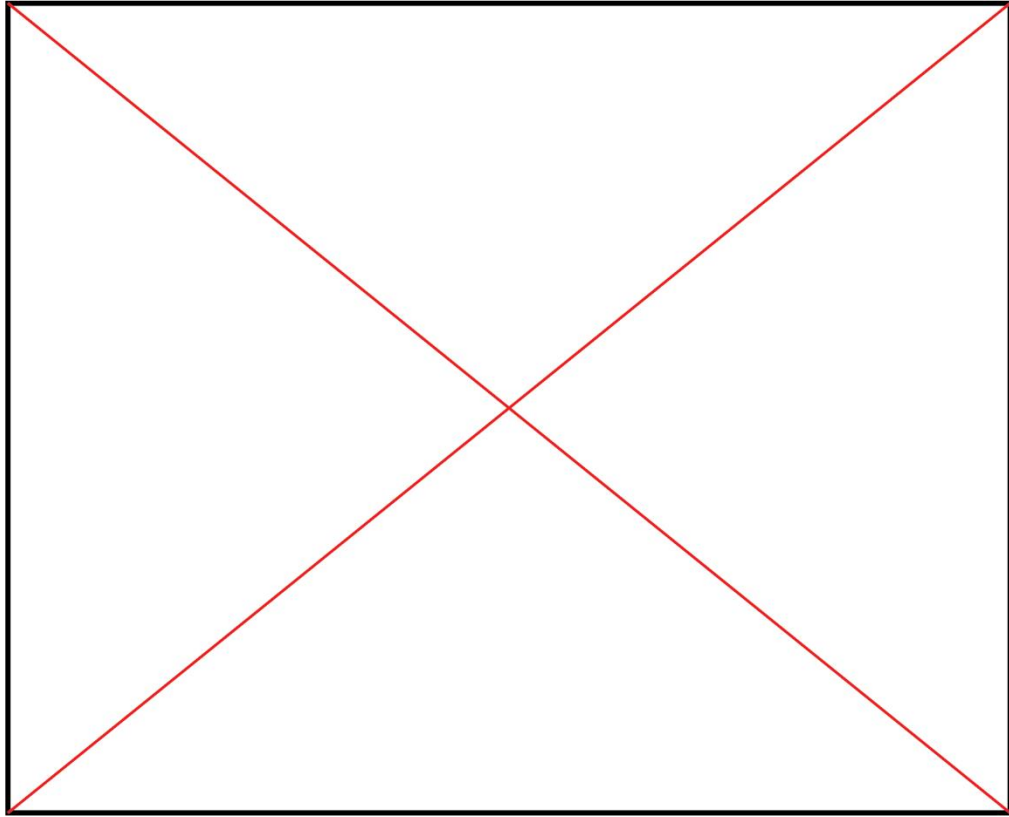
Figure 30. Output for the Non-Normalized Model showing high probability values in red and low probability values in green.

6.4 Model 2: Normalized and Weighted with Researcher Optimization

This model contained variables that were assigned differing weights of importance in the detection of karst features. Areas are displayed as a high probability (red and yellow) to low probability (greens) for karst feature development (Figure 31). Generally, this model predicts high karst probability as a band spanning from the northwest to the southeast, a reflection of the surface geology, the geologic contact between the Flowerpot Shale and the Medicine Lodge Gypsum, and topography.
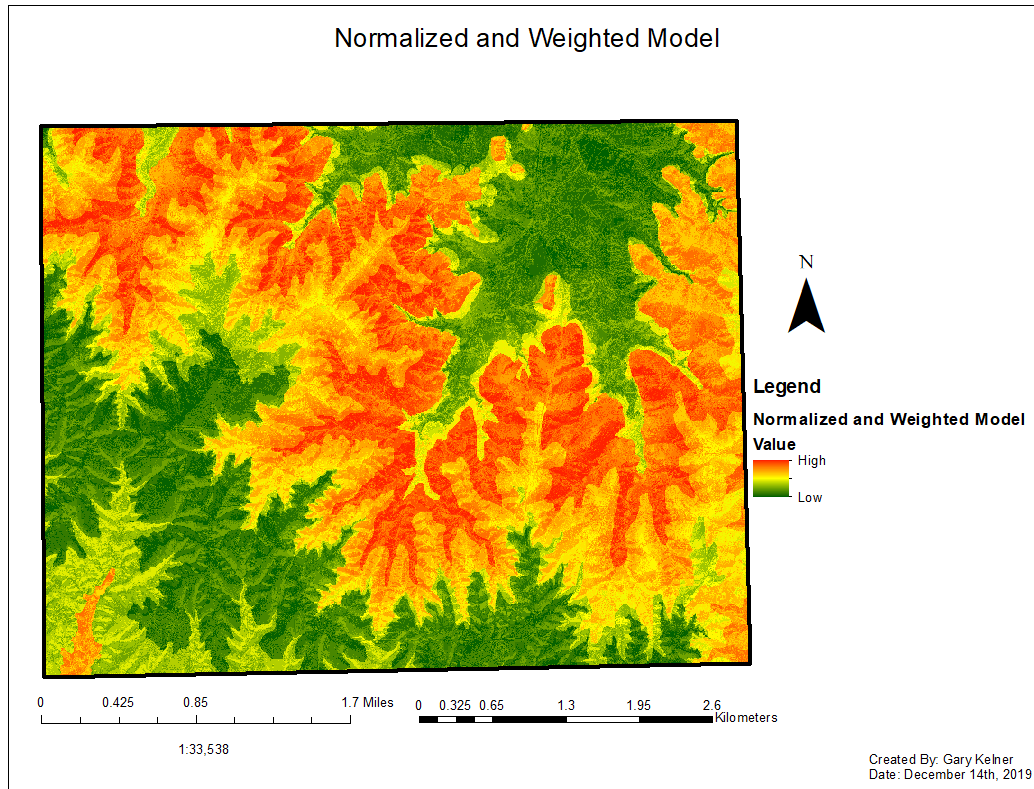
Figure 31. Output for the Normalized and Weighted Model showing high probability values in red and low probability values in green.

6.5   Agreement of the Two Models

Model 1 appeared to under-predict karst features, and model 2 appeared to over predict karst features; however, both models showed a high potential for karst prediction. Instead of using one model, the two models were combined into an agreement model. The two models were placed into the raster calculator to determine the agreement between models (Figure 32). This agreement model shows areas where both models agree in prediction of a karst feature (red; value =2), agree in the low probability of a karst feature (white; value =0), and where models do not agree in a karst feature (yellow;

value =1). Preference in selection of field validation points were given to high agreement (red; value=2) areas that intersected with sink-fill features.
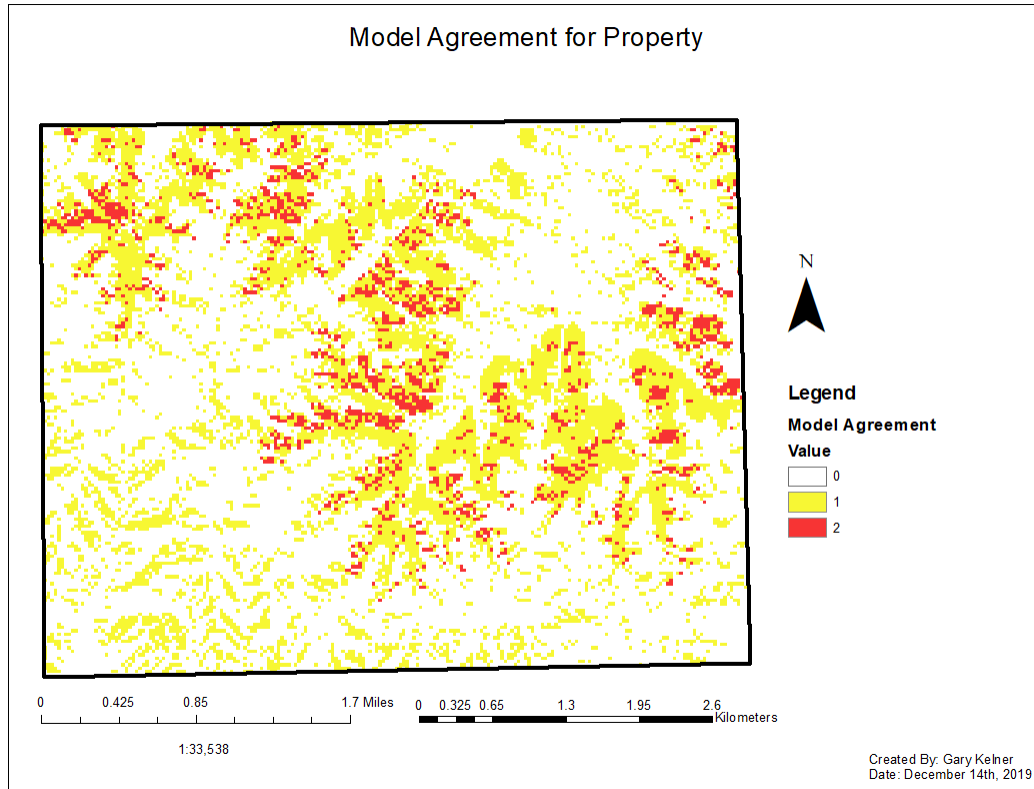
Figure 32. Model agreements between the two models that were generated map.

6.6   Model Field Validation

Of the 50 points selected for field validation (Figure 10), 26 points were verified as a karst feature, representing a 52% accuracy (Figure 33). In addition to visiting these points, areas near sink-fill indicated features with high model agreement were visited during field validation. This produced 12 additional karst features that did not appear as sink-fill features (Figure 33). Many of these features were either too small to be detected or cave entrances that do not have surface expression (valley entrances instead of sinkhole entrances). The combination of these points produced 38 total new karst features

that were added to the karst inventory of the property, increasing the number by 51% of the number of previously identified features (Figure 33).

Based on the results of these field validated models, the first hypothesis that the model would be more accurate than simply using the sink-fill function on the LiDAR DTM is correct. As indicated by the points in the northwest portion of the property, there are enclosed basins that are not sinkholes that have been identified by the sink-fill function. These points were falsely identified as potential karst features due to the errors associated with the geology shapefile. Additionally, the second hypothesis that karst features are associated with areas of higher vegetation density (indicated by NDVI) appears to be false. There is a narrow range in NDVI for among known karst features; however, this NDVI value was near zero (slightly positive) but not a higher vegetation density. Future studies should focus on climatic changes and their influence on NDVI among karst and non-karst areas.
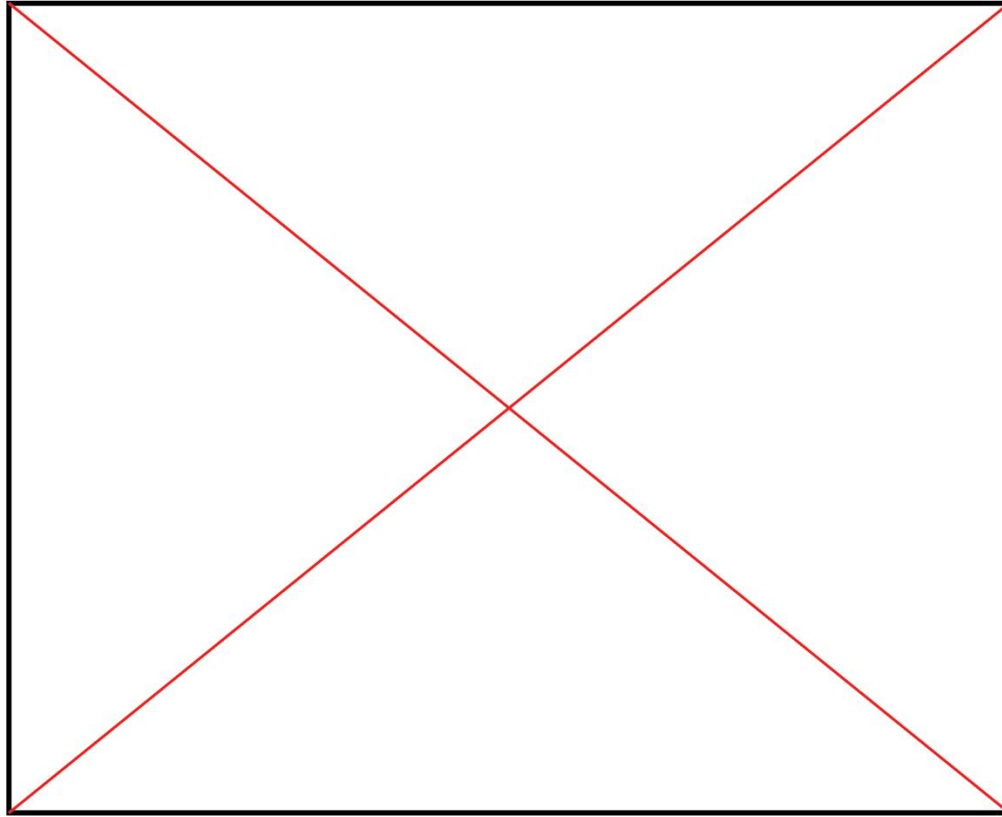
Figure 33. The verified, investigate and new karst points on the property.

6.7   Karst Hazard Map showing Vulnerability to Infrastructure

The identification of karst hazards to infrastructure on the property used the reclassified land cover/land use and the normalized (model 2) model (Figure 31). Most of the property shows a low vulnerability for hazards to infrastructure. The highest vulnerability (red) on the property occurs along roads and within drainage systems that have been artificially dammed to create cattle ponds. Moderate high (orange) values occur on slopes near roads, buildings, and valleys below dammed pond features. Future development of this property should avoid high and moderate high (red and orange) areas because of the increased hazard risk.
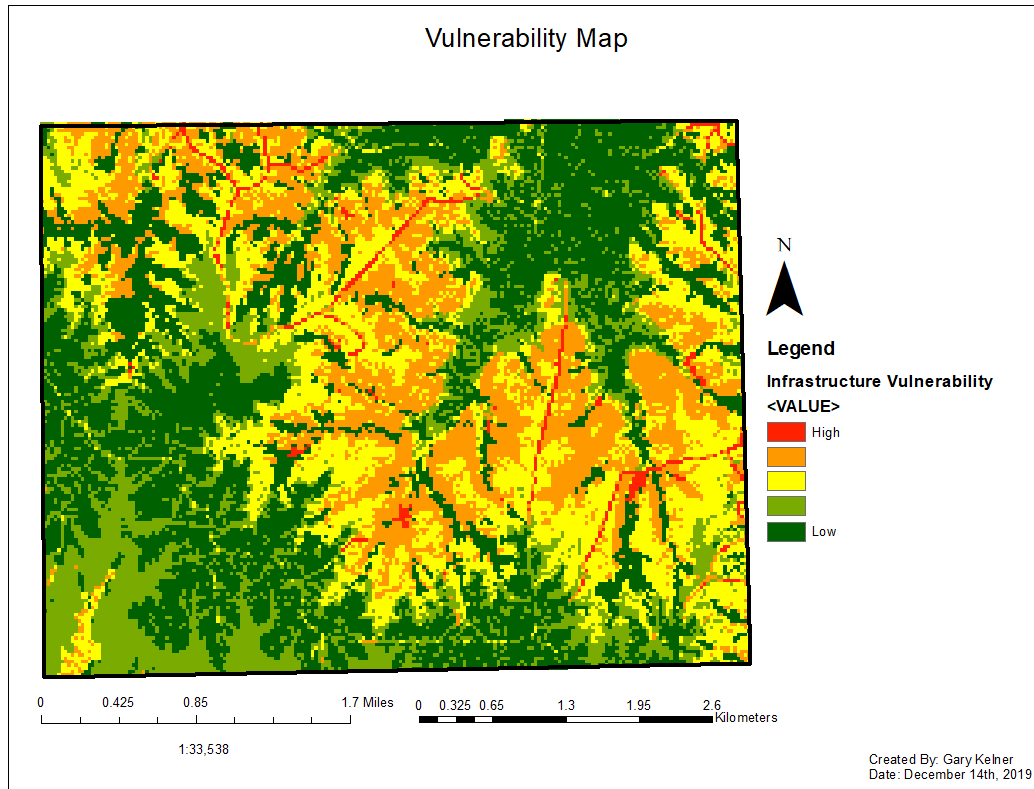
Figure 34. Study area vulnerability of karst features to infrastructure map.

6.8   Petrographic Results

Sample locations were predominately collected from the dolomitic layers within

caves (Figure 35). Samples were also collected from outcrops and non-cave karst features

(example: sinkholes) that appeared to contain similar dolomitic layers (Figure 35).

Twenty-five samples were collected for petrographic analyses. Seventeen samples were

collected from caves (Figure 36 A-B), and eight samples were collected from locations

that were not caves (Figure 36 C-D).
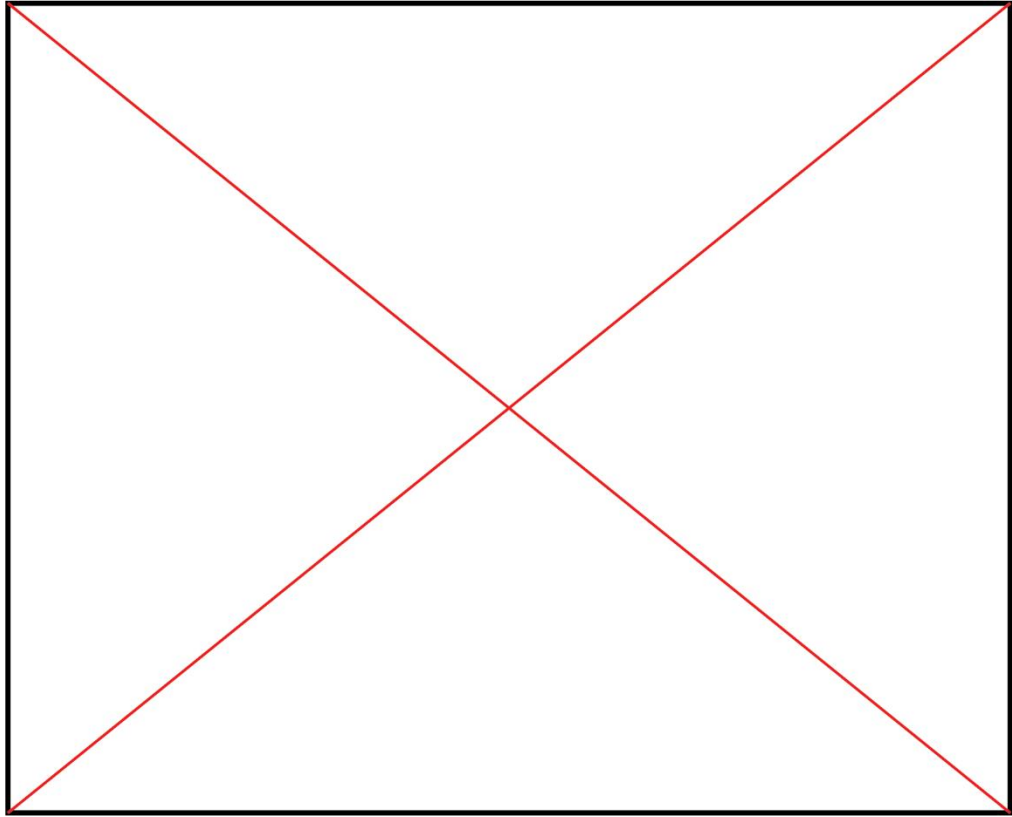
Figure 35. Study area sample collection locations from both caves (yellow) and non-cave

karst features (green).
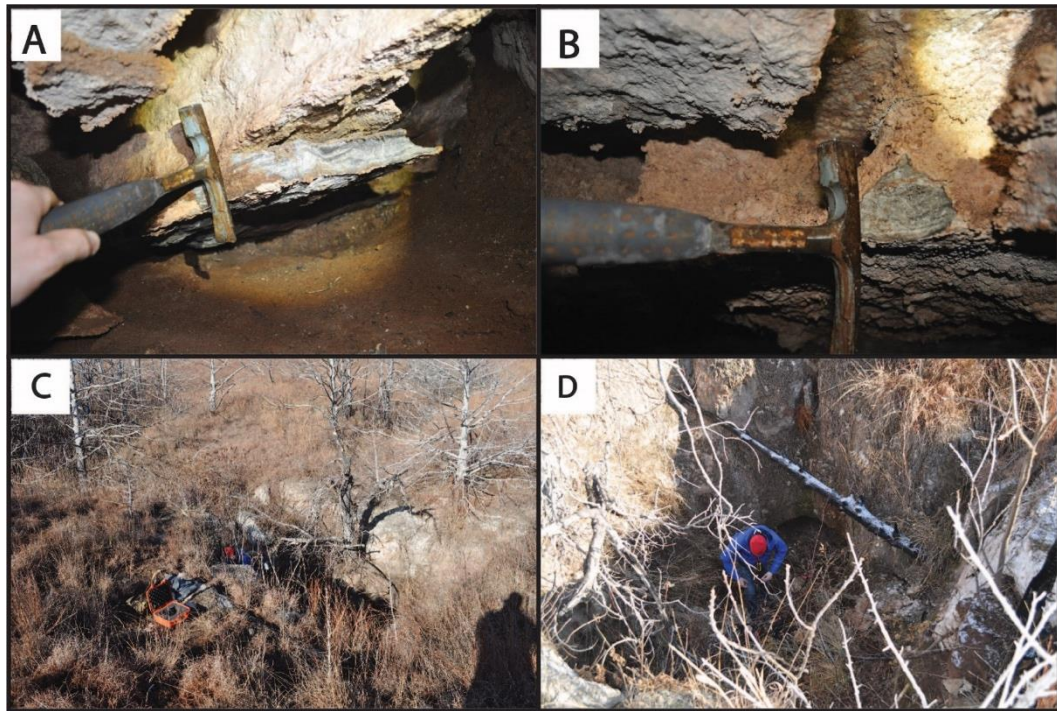
Figure 36. Sample collection photographs from cave ledges and sinkholes. Samples were either collected from rock ledges in caves (A and B) or from ledges exposed within sinkholes (C and D).

Dolomite was the dominant mineral identified in these samples based on point count statistics (Table 1). Dolomite ranged between 59% and 100%, and the maximum percentage of dolomite was 100%. Gypsum ranged between 0% and 32%, and the maximum percentage of gypsum was 32%. The dominant type of dolomite present was planar dolomite (Figure 37), and there was a very small percentage of pore space in the samples. The dominant allochems present were pellets and ooids, and minor fractures were found in several samples.

Table 1: The results of the point count analysis conducted on the petrographic thin sections within Barber County, Kansas.

Sample	Gypsum	% Gypsum	Gypsum Laths	% Gypsum Laths	Planar Dolomite	% Dolomite	% Pore	% Fracture
CC-2	0.0	0.0	13.0	13.0	87.0	87.0	0.0	0.0
CC-1	0.0	0.0	18.0	18.0	81.0	81.0	0.0	1.0
G6-2	0.0	0.0	3.0	3.0	97.0	97.0	0.0	0.0
G6-1	33.0	32.4	0.0	0.0	69.0	67.6	0.0	0.0
POND	15.0	14.9	0.0	0.0	86.0	85.1	0.0	0.0
YCAR-2	7.0	7.0	0.0	0.0	93.0	93.0	0.0	0.0
YCAR-1	4.0	4.0	0.0	0.0	96.0	96.0	0.0	0.0
UN-E	8.0	8.0	0.0	0.0	92.0	92.0	0.0	0.0
UN	0.0	0.0	0.0	0.0	107.0	100.0	0.0	0.0
CP-1	2.0	2.0	0.0	0.0	97.0	97.0	1.0	0.0
CP-2	4.0	4.0	0.0	0.0	96.0	96.0	0.0	0.0
CP-3	14.0	13.9	0.0	0.0	83.0	82.2	4.0	0.0
ACG-1	13.0	12.9	0.0	0.0	88.0	87.1	0.0	0.0
ACG-2	13.0	12.9	0.0	0.0	87.0	86.1	1.0	0.0
ACG-3	17.0	17.0	0.0	0.0	83.0	83.0	0.0	0.0
AC-1	3.0	3.0	0.0	0.0	97.0	97.0	0.0	0.0
352-1	0.0	0.0	0.0	0.0	100.0	100.0	0.0	0.0
352-2	0.0	0.0	0.0	0.0	100.0	100.0	0.0	0.0
SC-1	15.0	15.0	0.0	0.0	85.0	85.0	0.0	0.0
SC-2	3.0	3.0	0.0	0.0	97.0	97.0	0.0	0.0
SOC-1	1.0	1.0	0.0	0.0	99.0	99.0	0.0	0.0
SOC-2	0.0	0.0	0.0	0.0	100.0	100.0	0.0	0.0
MC-2	16.0	16.0	0.0	0.0	84.0	84.0	0.0	0.0
MC-1	41.0	41.0	0.0	0.0	59.0	59.0	0.0	0.0
PC-1	2.0	2.0	0.0	0.0	97.0	96.0	2.0	0.0

Two sedimentary facies were interpreted from the point count data: 1) Algal Mat facies (Figure 37) and 2) Peloidal (peldolomicrite) facies (Figure 38). The Algal Mat facies was defined as a dolobiolithite with repeating banding layers representing altering algal layers (Figure 37). This facies correlates to the interpreted lacustrine depositional environment for the Blaine Formation (Benison et al., 2015). The Peloidal facies was

characterized by pellets and ooids (Figure 38), and generally agreed with previous

petrographic studies of the Blaine Formation (Benison et al., 2015). The mineral

composition of these facies agree with (Gauvey, 2019), being composed of greater than

90% dolomite. Gypsum laths (Figure 39) in these samples is consistent with other studies

of the Medicine Lodge Gypsum (Benison et al., 2015). Some samples of the

peldolomicrite were intensely recrystallized by the dolomitization process, which nearly

completely destroyed the original depositional fabric (Figure 40).
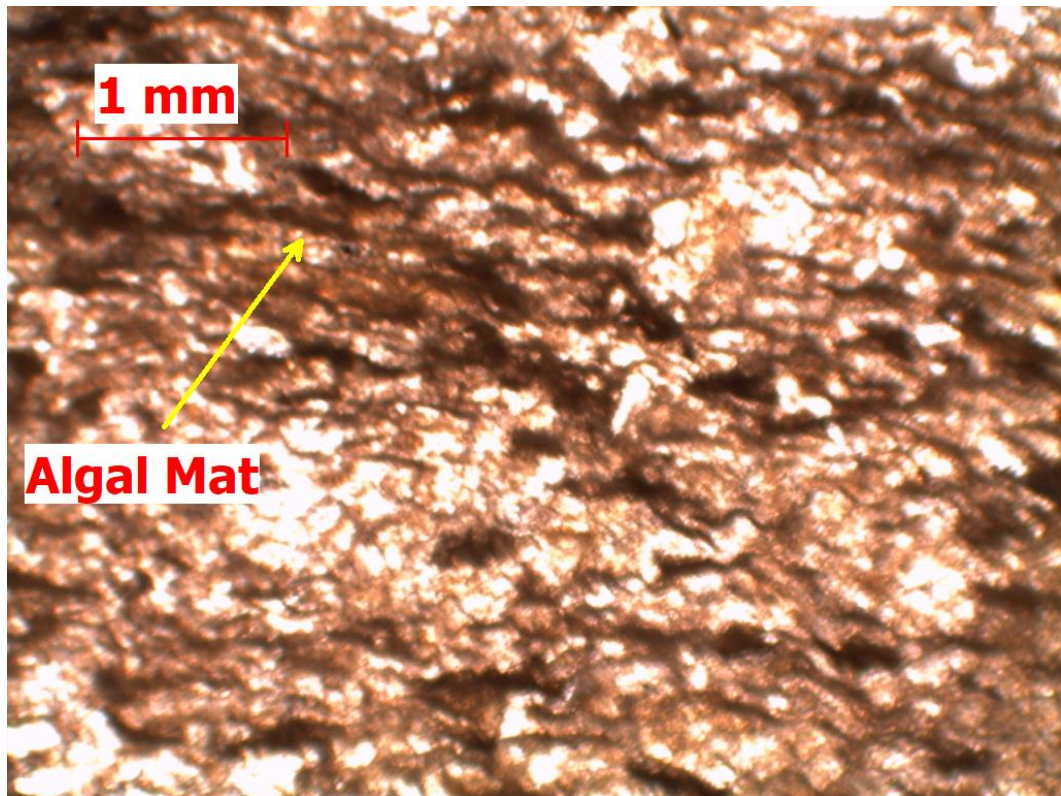
Figure 37. Sample PC1 in Plain Polarized Light using the 4x objective showing the Algal
Mat facies.
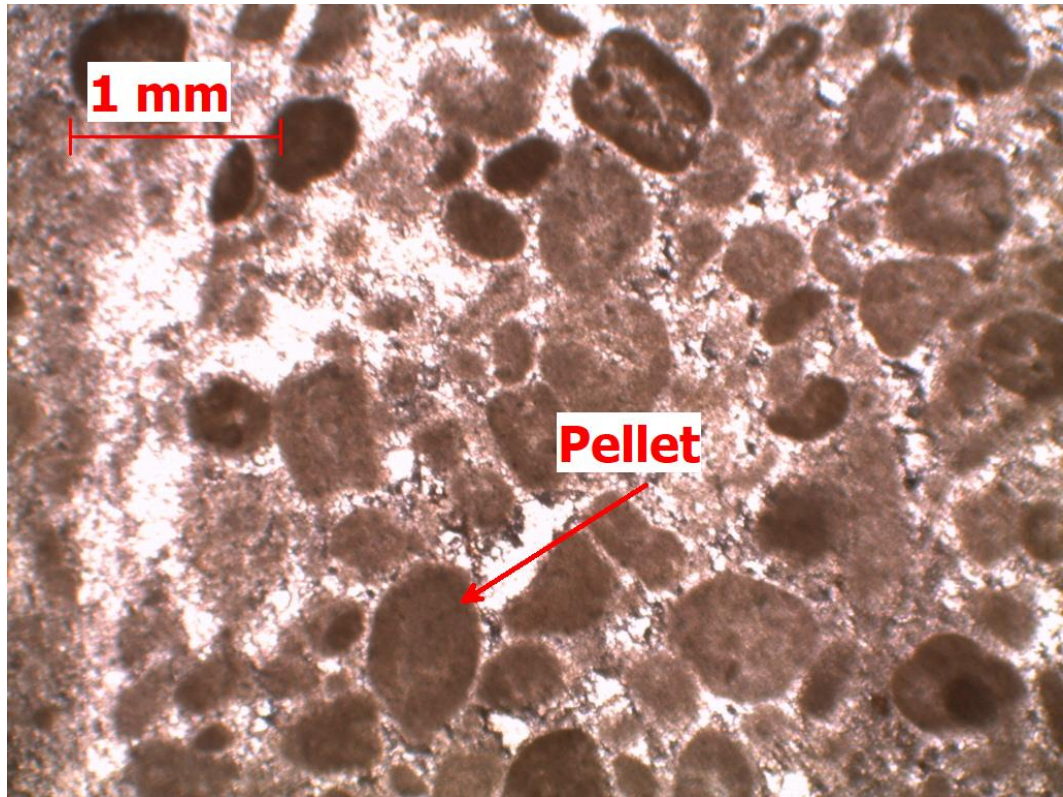
Figure 38. Sample SC1 in Plain Polarized Light using the 4x objective showing the

Pelloid facies.
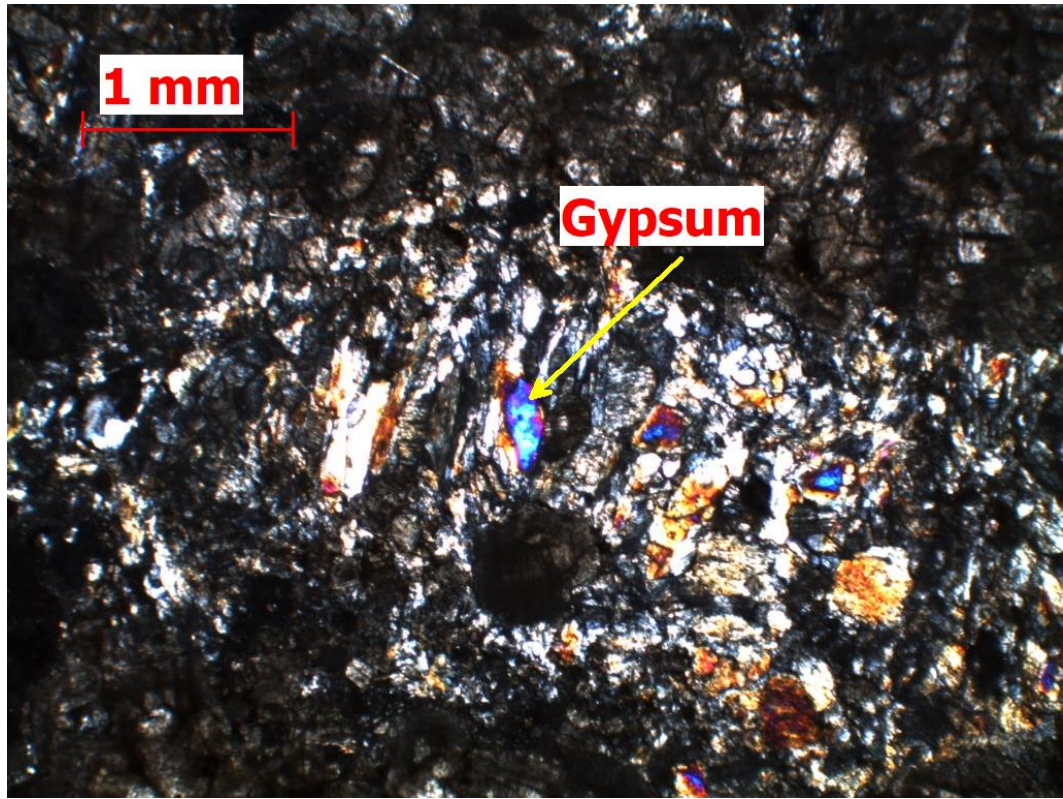
Figure 39. Sample showing gypsum laths in thin section from sample CC-2 in crossed polarized light using the 4x objective.
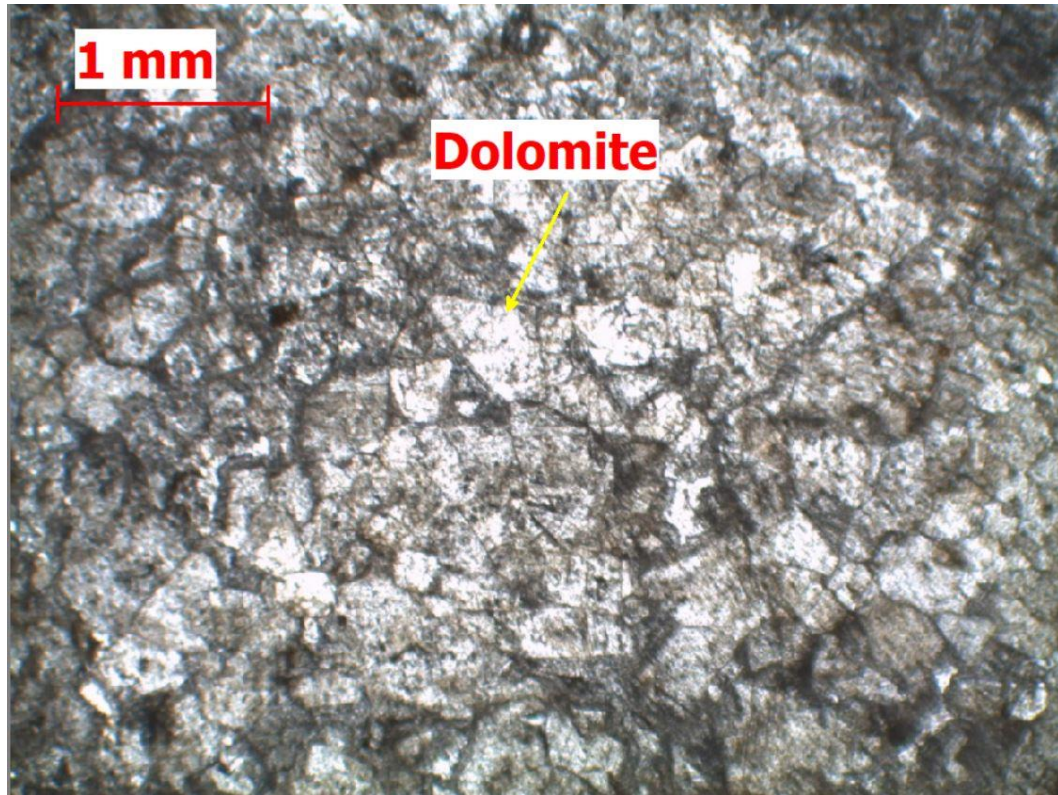
Figure 40. Sample UNE in Plain Polarized Light showing the dolomitization in Plain Polarized Light using the 4x objective.

Because of the sporadic nature of outcrops on the property, continuous sampling of the dolomitic layers was not possible. It was also impossible to determine if more than one dolomitic layer existed at the local scale on the property (i.e. there were not any significant vertical sections of exposure that existed on the property and/or core drilling data on the property to access if multiple dolomitic strata exists in the sequence). The location of samples with their corresponding facies was plotted to determine if these dolomitic layers represent a single stratigraphic layer that extends across the property or if they represent multiple stratigraphic layers that contribute to karst formation (Figure 41). Additionally, samples from caves and other karst features were examined to determine if a single facies existed in those samples (Table 2).
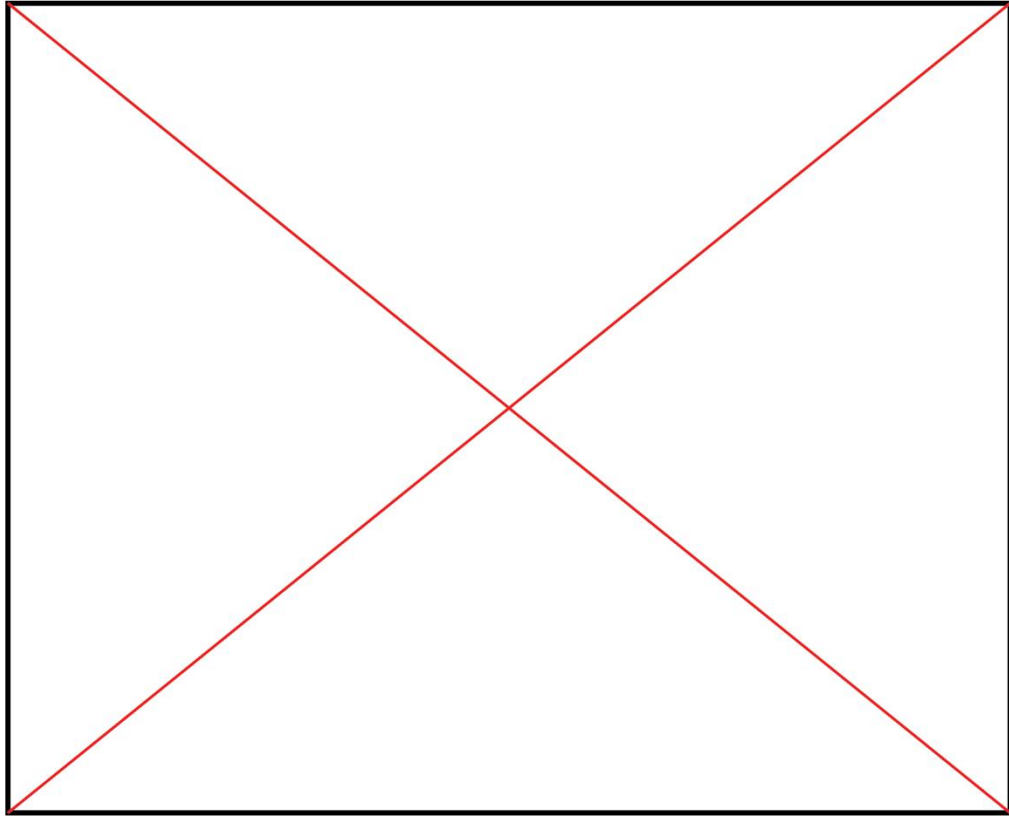
Figure 41. Study area classified facies plotted map.

Table 2. Sedimentary facies of samples from karst features.

Feature Name	Facies Identified
Acorn	Peloidal
CC	Algal Mat
CP	Peloidal
Dolomite	Peloidal
G6	Peloidal
Monkey	Algal Mat
Pond	Peloidal
Proto-Cond	Algal Mat
Scared	Peloidal
Second Opp	Peloidal
U-Turn	Algal Mat
Y-intersection	Peloidal

The distribution of these two facies are not uniform across the property, with some samples in extremely close proximity having different facies (Figure 41). The change in sedimentary facies could be attributed to gradual changes in the environment during deposition; however, it would produce a distribution that varies across the property from one facies to the other. Additionally, there were no samples that displayed transitional depositional facies that were identified. When the distribution of the facies is closely examined, there are several samples of differing facies that plot near each other (Figure 41). This has been interpreted to represent multiple stratigraphic layers on the property, instead of a single layer that varies in facies.

Gauvey (2019) interpreted the dominant karst forming process in this region as the product of differential dissolution between gypsum and dolostone until the underlying Flowerpot Shale Formation is mechanically eroded. Therefore, Gauvey (2019) interpreted the presence of caves on this property as an indicator of the contact between the Medicine Lodge Gypsum and the Flowerpot Shale. Conversely, these findings suggest that there are multiple dolomitic strata within the lower Medicine Lodge Gypsum that lead to the development of karst features.

To determine the stratigraphic elevation of these two strata, elevations were extracted from the LiDAR data using zonal statistics of the sample locations (Table 3). The Algal Mat facies occurs between 559.0 meters and 564.4 meters, and the Peloidal facies occurs between 559.8 meters and 571.8 meters. There is considerable overlap between the elevation of these samples, which may be due to one of the following: 1) stratigraphic dip across the property, 2) error associated with using a handheld GPS for recording locations of cave entrances, 3) using cave entrance as location point when

73

sample was located within the cave (sometimes 10s of meters from the entrance), or 4)

the existence of only a single stratigraphic layer. Explanation #4 is unlikely because of

the relative close proximity of several samples with different facies as mentioned above.

Explanations 1-3 are all possible, making these elevations highly questionable for their

accuracy. However, it is clear that the Algal Mat facies occurs at a lower elevation

relative to the Peloidal facies. Therefore, it is interpreted that the Algal Mat facies

represents the contact between the Medicine Lodge Gypsum and the underlying

Flowerpot Shale, while the Peloidal facies represents a slightly higher stratigraphic

dolomitic layer. Both of these dolomitic layers are likely the previously identified Cedar

Springs Dolomite (Fay, 1964) and are integral in the karst formation process. Based on

these results, the hypothesis that a single petrographically uniform layer exists that

controls karst formation on this property is false.

Table 3: The elevations of karst feature samples and their respective geologic facies.

Name	Facies	Elevation (m)
Acorn	Peloidal	564.6
CC	Algal Mat	564.6
CP	Peloidal	561.5
Dolomite	Peloidal	559.8
G6	Peloidal	561.9
Monkey	Algal Mat	560.7
Opportunity	Peloidal	565.7
Pond	Peloidal	563.3
Proto-Cond	Algal Mat	559.0
Scared	Peloidal	565.7
U-Turn	Algal Mat	564.3
Y-Intersection	Peloidal	571.8

CHAPTER VII

SUMMARY & CONCLUSIONS

7.1   Chapter Overview

This chapter summarizes the main findings and conclusions of this thesis. First, the predictive models, their accuracy, and their use to create vulnerability maps are summarized. Next, the limitations and future work using these models are summarized. Finally, the petrographic analyses in this area are summarized.

7.2   Predictive Models

Overall, the models created during this thesis were successful in the prediction of karst features on this property. Features of interest were identified from the sink-fill feature using LiDAR data and the satellite imagery. Features were selected based on the intersection of these features of interest with the model output. Model success was measured by the ability of positive identification of these features during field validation. Models erroneously predicted high karst probability in the northwestern portion of the property; however, this was a by-product of inaccurate data (misidentified geologic layers) that was input into the models. Correction of inaccurate data should be the focus of future geologic studies on the property.

In future iterations of the model, the following are some things that could be altered to make the model run more smoothly and have a higher accuracy of karst feature prediction. First, higher resolution aerial/satellite imagery of the area could be used with multiple bands to detect landscape features. The higher resolution imagery would aid in the field reconnaissance and the ability to identify surface karst features from the

imagery. Finally, higher resolution LiDAR that is smaller than one meter in resolution could be obtained to increase detection of karst features.

There were multiple limitations that came up when field validating the model for karst features. One limitation was that the geology on the northwest portion of the study area was incorrectly mapped/interpreted by the data source. The geologic unit that was seen in this area was not a karst-bearing unit, instead it appeared to be Quaternary loess or sandstone. The geology needs to be correctly identified at the scale of the property before using in any future predictive models.

The use of this predictive model can assist landowners and city planners for hazard mitigation, preventing future structural damage, potential agricultural and livestock loss, and siting where to put water restrictive features such as dams. Karst features are one of the most highly vulnerable landforms on the planet, can harbor species unknown to science, and should be observed under secure conditions where only select individuals are allowed to enter the cave. Knowing the potential location of karst features allows landowners to prevent the destruction of these fragile habitats. Additionally, these models could be used by other agencies that need assistance in the prediction of karst features in gypsum areas of Kansas.

7.3   Petrographic Conclusions

Two sedimentary facies were discerned from the group of samples. The first facies distinguished from the samples was the Algal Mat facies. This facies was defined as having alternating layers of dolomitized micrite that can be seen in petrographic thin section. The second facies was classified as a Peldolomicrite (Peloidal) facies. In addition

76

to pelloids, this facies contained ooids in petrographic thin section. These sedimentary facies generally agreed with previous studies (Benison et al., 2015; Gauvey, 2019). These dolomitic layers have been interpreted to represent the base of the Medicine Lodge Gypsum and contribute significantly to karst formation on the property (Benison et al., 2015; Gauvey, 2019). The results of this study suggested that there are two stratigraphic layers present in caves and associated with karst features on the property. The exact elevation of these stratigraphic layers was unable to be determined accurately; however, the relative position placed the Algal Mat facies below the Peloidal facies. This suggests that there were multiple stratigraphic layers responsible for karst formation, not only the basal carbonates suggested by Gauvey (2019). Future studies to determine the accurate elevation of these layers should be conducted to determine the exact stratigraphic location.

LITERATURE CITED

Abdullah, T.Y., Watney, W.L., Walton, A.W. and Doveton, J.H., 1985. Depositional facies in the Funston cycle (Lower Permian) of southwestern Kansas. *Core studies in Kansas—sedimentology and diagenesis of economically important rock strata in Kansas, Watney, WL, Walton, AW, and Doveton, JH, eds.: Kansas Geological Survey, Subsurface Geology Series*, *6*, pp.161-171.

Angel, J.C., Nelson, D.O. and Panno, S.V., 2004. Comparison of a new GIS-based technique and a manual method for determining sinkhole density: An example from Illinois' sinkhole plain. Journal of Cave and Karst Studies, 66(1), pp.9-17.

Bates, R.L. and Jackson, J.A., 1987. Glossary of Geology: American Geological Institute. Alexandria, Virginia, 788.

Benison, K.C. and Goldstein, R.H., 2001. Evaporites and siliciclastics of the Permian Nippewalla Group of Kansas, USA: a case for non-marine deposition in saline lakes and saline pans. Sedimentology, 48(1), pp.165-188.

Benison, K.C., Zambito IV, J.J. and Knapp, J., 2015. Contrasting siliciclastic–evaporite strata in subsurface and outcrop: an example from the Permian Nippewalla Group of Kansas, USA. Journal of Sedimentary Research, 85(6), pp.626-645.

Bischoff, J.L., Juliá, R., Shanks III, W.C. and Rosenbauer, R.J., 1994. Karstification without carbonic acid: Bedrock dissolution by gypsum-driven dedolomitization. Geology, 22(11), pp.995-998.

Conrad, O., Bechtel, B., Bock, M., Dietrich, H., Fischer, E., Gerlitz, L., Wehberg, J., Wichmann, V., and Böhner, J. (2015): System for Automated Geoscientific Analyses (SAGA) v. 2.1.4, Geosci. Model Dev., 8, 1991-2007, doi:10.5194/gmd-8-1991-2015.

Cornelius, S.C., Sear, D.A., Carver, S.J. and Heywood, D.I., 1994. GPS, GIS and geomorphological field work. *Earth Surface Processes and Landforms*, *19*(9), pp.777-787.

Cragin, F. W., 1896. The Permian System in Kansas: Colorado College Studies, v. 6, p. 1-48.

Doctor, D.H. and Young, J.A., 2013. An evaluation of automated GIS tools for delineating karst sinkholes and closed depressions from 1-meter LIDAR-derived digital elevation data.

Fay, R. O., 1964. The Blaine and related formations of northwestern Oklahoma and southern Kansas: Oklahoma Geol. Survey, Bull. 98, 238 p.

Ford, D.C. and Williams, P.W., 1989. Karst geomorphology and hydrology (Vol. 601). London: Unwin Hyman.

Galve, J.P., Gutiérrez, F., Remondo, J., Bonachea, J., Lucha, P. and Cendrero, A., 2009. Evaluating and comparing methods of sinkhole susceptibility mapping in the Ebro Valley evaporite karst (NE Spain). Geomorphology, 111(3-4), pp.160-172.

Gauvey, K., 2019. Gypsum Karst Speleogenesis in Barber County, Kansas of the Permian Blaine Formation.

Gauvey, K.L.; and Sumrall, J.B., 2018, Gypsum Karst Reconnaissance In Barber County, Kansas of the Permian Blaine Formation: Geological Society of America Abstracts with Programs, v.50, no.6.

Guth, P.L., 2009, Geomorphometry in MICRODEM, In Hengl, T., Reuter, H.I. (eds), Geomorphometry: concepts, software, applications. Developments in Soil Science Series, Elsevier, ISBN-13: 978-0-12-374345-9, p.351-366.

Gutierrez, F., Cooper, A.H. and Johnson, K.S., 2008. Identification, prediction, and mitigation of sinkhole hazards in evaporite karst areas. Environmental Geology, 53(5), pp.1007-1022.

Ham, W. E., 1960. Middle Permian evaporites in southwestern Oklahoma: Internat. Geol. Congress, 21 St., Norden, Rept. Pt. 12, p. 138-151.

Hills, J. M., 1942. Rhythm of Permian seas--a paleogeographic study: Am. Assoc. Petrol. Geologists, Bull., v. 26, p. 217-255.

Hubbard, Jr, D.A., 2003. Use of regional sinkhole mapping for sinkhole susceptibility maps. In Sinkholes and the Engineering and Environmental Impacts of Karst (pp. 61-71).

Hutchison, C.S., 1974, Laboratory Handbook of Petrographic Techniques: New York, NY, John Wiley & Sons Inc.

Hyland, S.E., 2005. Analysis of sinkhole susceptibility and karst distribution in the northern Shenandoah Valley, Virginia: implications for low impact development (LID) site suitability models (Doctoral dissertation, Virginia Tech).

Johnson, K.S. (1967). Stratigraphy of the Permian Blaine Formation and associated strata

in southwestern Oklahoma [PhD dissertation]. Champaign (IL): University of

Illinois. 247 p.

Johnson, K.S., 1997. Evaporite karst in the United States. Carbonates and

Evaporites, 12(1), pp.2-14.

Karacan, E. and Yılmaz, I., 1997. Collapse dolines in Miocene gypsum: an example from

SW Sivas (Turkey). Environmental Geology, 29(3-4), pp.263-266.

Klimchouk, A., 1996. The dissolution and conversion of gypsum and

anhydrite. *International Journal of Speleology*, *25*(3), p.2.

Kresic, N., 2013, Water in Karst: management, vulnerability, and restoration: New York,

McGraw-Hill.

Kulstad, R. O.; Fairchild, P.; and McGregor, D., 1956. Gypsum in Kansas: Kansas Geol.

Survey. Bull. 113, 110 P.

Moore, R. C.; and others., 1951. The Kansas rock column: Kansas Geol. Survey, Bull.

89, p. 1-132.

Norton, G.H., 1939. Permian red beds of Kansas: American Association of Petroleum

Geologists, Bulletin, v. 23, p. 1751–1819.

Ourhzif, Z., Algouti, A. and Hadach, F., 2019. Lithological mapping using Landsat 8 oli

and aster multispectral data in imini-ounilla district south high atlas of

Marrakech. *International Archives of the Photogrammetry, Remote Sensing &*

Spatial Information Sciences.

81

Ozdemir, A., 2016. Sinkhole susceptibility mapping using logistic regression in
 Karapınar (Konya, Turkey). Bulletin of Engineering Geology and the
 Environment, 75(2), pp.681-707.

Palmer, A.N., 2007. Cave geology (Vol. 454). Dayton: Cave books.

Plummer, N. and Back, W., 1980. The mass balance approach: application to interpreting
 the chemical evolution of hydrologic systems. *American Journal of
 Science*, *280*(2), pp.130-142.

Rahimi, M. and Alexander Jr, E.C., 2013. Locating sinkholes in LiDAR coverage of a
 glacio-fluvial karst, Winona County, MN.

Raines, M.A. and Dewers, T.A., 1997. Dedolomitization as a driving mechanism for karst
 generation in Permian Blaine Formation, Southwestern Oklahoma,
 USA. Carbonates and Evaporites, 12(1), pp.24-31.

Raines, M.A. and Dewers, T.A., 1997. Mixed transport/reaction control of gypsum
 dissolution kinetics in aqueous solutions and initiation of gypsum karst. Chemical
 Geology, 140(1-2), pp.29-48.

Schillaci, C., Braun, A. and Kropáček, J., 2015. 2.4. 2. Terrain analysis and landform
 recognition. Geomorphological Techniques (Online Edition).

Seale, L.D., Florea, L.J., Vacher, H.L. and Brinkmann, R., 2008. Using ALSM to map
 sinkholes in the urbanized covered karst of Pinellas County, Florida—1,
 methodological considerations. Environmental Geology, 54(5), pp.995-1005.

Siart, C., Bubenzer, O. and Eitel, B., 2009. Combining digital elevation data (SRTM/ASTER), high resolution satellite imagery (Quickbird) and GIS for geomorphological mapping: A multi-component case study on Mediterranean karst in Central Crete. Geomorphology, 112(1-2), pp.106-121.

Siegal, B.S., Barry, S., II, G. and Allan, R., 1980. Remote sensing in geology/ed. by Barry S. Siegal and Alan R. Gillespie (No. 550 S5.).

Swineford, A., 1955. Petrography of Upper Permian rocks in south-central Kansas: Kansas Geol. Survey, Bull., 111, 179 p.

Theilen-Willige, B., Malek, H., Charif, A., El Bchari, F. and Chaïbi, M., 2014. Remote sensing and GIS contribution to the investigation of karst landscapes in NW-Morocco. Geosciences, 4(2), pp.50-72.

Tucker, M.E. ed., 2009. *Sedimentary petrology: an introduction to the origin of sedimentary rocks*. John Wiley & Sons.

Wade, T. and Sommer, S., 2006. *A to Z GIS, An illustrated dictionary of geographic information systems*. Esri Press.

Waltham, T., Waltham, A.C., Bell, F.G. and Culshaw, M.G., 2005. Sinkholes and subsidence: karst and cavernous rocks in engineering and construction. Springer Science & Business Media.

White, W.B., 1988. *Geomorphology and hydrology of karst terrains* (No. 551.447 W4).

Yilmaz, I., 2007. GIS-based susceptibility mapping of karst depression in gypsum: a case study from Sivas basin (Turkey). Engineering Geology, 90(1-2), pp.89-103.

Yilmaz, I., Marschalko, M. and Bednarik, M., 2011. Gypsum collapse hazards and the importance of hazard mapping. Carbonates and Evaporites, 26(2), pp.193-209.

Young, J., and Beard, J. (1993). Caves in Kansas, Kansas Geological Survey, Educational Series 9.

APPENDICES

See the following pages.

(Left Intentionally Blank)

APPENDIX A: Zonal Statistics Slope Table

OBJECTID	OBJECTID_1	COUNT	AREA	MIN	MAX	RANGE	MEAN	STD	SUM
1	1	53098	13274.5	0.1006	60.1339	60.033	14.7289	8.489	782076.9808
2	2	146762	36690.5	0.0469	77.133	77.086	14.0721	9.909	2065247.922
3	3	31301	7825.25	0.1005	50.6019	50.501	11.3034	6.917	353809.2221
4	4	31295	7823.75	0.0271	78.1654	78.138	14.2032	10.48	444490.1587
5	5	65470	16367.5	0.0403	77.1265	77.086	14.8716	12.77	973645.8667
6	6	31308	7827	0.1608	75.7951	75.634	20.4185	12.61	639263.0055
7	7	31314	7828.5	0.189	70.2983	70.109	17.3974	14.25	544782.6131
8	8	31318	7829.5	0.0228	32.3989	32.376	6.06072	3.854	189809.4858
9	9	40068	10017	0.0919	69.8317	69.74	17.119	10.7	685922.2365
10	10	31296	7824	0.212	43.2549	43.043	13.3775	4.719	418661.7172
11	12	95539	23884.75	0.0819	56.6282	56.546	12.0722	8.58	1153361.409
12	13	49690	12422.5	0.05	75.68	75.63	16.72	14.13	830,611.34
13	15	34120	8530	0.12	65.38	65.26	9.50	8.01	324,181.46
14	16	31310	7827.5	0.05	72.89	72.84	10.20	9.94	319,354.39
15	17	31313	7828.25	0.04	60.26	60.22	15.53	11.06	486,331.98
16	18	134703	33675.75	0.01	74.68	74.67	14.65	12.42	1,973,596.59
17	22	41804	10451	0.09	60.51	60.42	11.39	9.09	476,085.39
18	23	31303	7825.75	0.04	64.38	64.34	10.92	7.91	341,699.54
19	24	35428	8857	0.05	57.85	57.80	17.41	11.68	616,929.68
20	25	31300	7825	0.04	65.65	65.61	10.70	9.92	334,996.06
21	26	41441	10360.25	0.04	71.93	71.90	17.88	16.06	740,845.62
22	27	31307	7826.75	0.21	66.72	66.50	20.15	11.71	630,895.73
23	28	47555	11888.75	0.04	61.46	61.42	14.29	12.86	679,624.47
24	29	31309	7827.25	0.06	32.87	32.81	6.16	3.45	192,869.26

APPENDIX B: Zonal Statistics Elevation Table

OBJECTID	OBJECTID_1	COUNT	AREA	MIN	MAX	RANGE	MEAN	STD	SUM
1	1	53098	13274.5	554.30	575.75	21.45	564.28	4.24	29962401.55
2	2	146762	36690.5	553.20	588.98	35.78	571.92	7.14	83935774.25
3	3	31301	7825.25	551.85	567.38	15.53	560.26	4.62	17536807.98
4	4	31295	7823.75	546.43	565.94	19.52	557.65	5.27	17451524.30
5	5	65470	16367.5	555.08	575.70	20.61	567.67	5.15	37165162.55
6	6	31308	7827	552.06	577.34	25.28	566.14	4.40	17724729.92
7	7	31314	7828.5	556.77	578.40	21.63	569.07	4.16	17819830.07
8	8	31318	7829.5	588.10	593.97	5.87	590.73	1.30	18500526.82
9	9	40068	10017	556.73	576.48	19.75	565.40	4.11	22654637.50
10	10	31296	7824	565.47	581.11	15.63	573.76	3.49	17956535.26
11	12	95539	23884.75	530.45	561.33	30.89	547.55	8.56	52312231.82
12	13	49690	12422.5	554.11	573.15	19.04	564.37	3.44	28043339.88
13	15	34120	8530	555.80	570.25	14.45	566.11	2.61	19315581.69
14	16	31310	7827.5	530.86	546.80	15.93	540.81	3.62	16932804.64
15	17	31313	7828.25	549.66	571.53	21.87	560.08	7.16	17537757.95
16	18	134703	33675.75	554.50	573.99	19.49	566.98	4.26	76374250.90
17	22	41804	10451	544.22	561.07	16.85	555.67	3.11	23229241.84
18	23	31303	7825.75	563.32	579.08	15.76	572.76	3.69	17929189.43
19	24	35428	8857	550.78	575.91	25.13	565.28	8.28	20026889.41
20	25	31300	7825	555.69	570.11	14.42	565.55	2.36	17701727.51
21	26	41441	10360.25	536.55	558.32	21.76	551.08	5.95	22837234.73
22	27	31307	7826.75	560.06	579.09	19.03	570.14	4.46	17849338.89
23	28	47555	11888.75	552.92	571.70	18.78	566.44	3.86	26937034.41
24	29	31309	7827.25	566.34	575.30	8.96	571.76	1.67	17901113.94

APPENDIX C: Zonal Statistics Aspect Table

COUNT	AREA	MIN	MAX	RANGE	MEAN	STD	SUM
53098	13274.5	0.04	359.58	359.53	121.52	54.74	6452545.45
146762	36690.5	0.00	359.99	359.99	143.63	81.57	21079675.62
31301	7825.25	0.00	359.99	359.99	112.62	131.71	3525254.19
31295	7823.75	0.02	359.99	359.98	213.82	135.88	6691631.62
65470	16367.5	0.00	360.00	360.00	141.58	83.65	9269189.55
31308	7827	0.01	360.00	359.99	200.63	124.44	6281244.90
31314	7828.5	0.00	359.98	359.98	190.64	125.29	5969655.30
31318	7829.5	0.05	359.99	359.94	140.30	92.11	4393782.00
40068	10017	0.03	359.99	359.96	217.99	110.96	8734335.26
31296	7824	0.13	359.92	359.78	195.40	110.55	6115094.65
95539	23884.75	0.00	359.99	359.99	146.36	121.94	13983022.03
49690	12422.5	0.00	359.88	359.88	185.45	104.77	9215022.48
34120	8530	0.00	359.99	359.99	163.59	125.23	5581765.00
31310	7827.5	0.02	359.99	359.98	83.48	99.06	2613718.88
31313	7828.25	0.01	359.96	359.95	115.89	78.36	3628926.22
134703	33675.75	0.00	359.99	359.99	146.54	99.91	19738728.39
41804	10451	0.02	359.98	359.96	193.47	113.55	8087897.92
31303	7825.75	0.01	359.99	359.98	232.53	129.91	7278945.30
35428	8857	0.00	359.93	359.93	126.87	88.77	4494841.79
31300	7825	0.08	359.86	359.77	157.85	67.25	4940750.75
41441	10360.25	0.00	359.98	359.98	218.53	92.66	9056215.32
31307	7826.75	0.00	359.97	359.97	203.93	94.40	6384512.68
47555	11888.75	0.03	359.98	359.95	209.91	82.98	9982082.39
31309	7827.25	0.03	359.98	359.95	256.07	82.05	8017303.85

APPENDIX D: Zonal Statistics NDVI Table

OBJECTID	COUNT	AREA	MIN	MAX	RANGE	MEAN	STD	SUM
1	14	12600	0.02	0.02	0.00	0.02	0.00	0.24
2	40	36000	0.01	0.03	0.01	0.02	0.00	0.79
3	9	8100	0.01	0.02	0.00	0.01	0.00	0.13
4	8	7200	0.02	0.02	0.00	0.02	0.00	0.13
5	17	15300	0.02	0.03	0.01	0.02	0.00	0.37
6	9	8100	0.02	0.02	0.00	0.02	0.00	0.16
7	9	8100	0.02	0.02	0.00	0.02	0.00	0.17
8	8	7200	0.01	0.02	0.01	0.02	0.00	0.13
9	12	10800	0.02	0.02	0.01	0.02	0.00	0.23
10	9	8100	0.02	0.02	0.00	0.02	0.00	0.19
11	24	21600	0.01	0.02	0.01	0.02	0.00	0.43
12	14	12600	0.02	0.02	0.01	0.02	0.00	0.25
13	9	8100	0.02	0.02	0.00	0.02	0.00	0.16
14	9	8100	0.01	0.02	0.00	0.02	0.00	0.15
15	8	7200	0.02	0.02	0.01	0.02	0.00	0.14
16	40	36000	0.01	0.02	0.01	0.02	0.00	0.67
17	12	10800	0.02	0.02	0.00	0.02	0.00	0.21
18	9	8100	0.01	0.02	0.01	0.02	0.00	0.17
19	12	10800	0.01	0.02	0.00	0.02	0.00	0.18
20	8	7200	0.02	0.02	0.00	0.02	0.00	0.14
21	11	9900	0.01	0.02	0.00	0.02	0.00	0.17
22	8	7200	0.02	0.02	0.00	0.02	0.00	0.15
23	13	11700	0.01	0.02	0.00	0.02	0.00	0.20
24	8	7200	0.02	0.02	0.00	0.02	0.00	0.15

APPENDIX E: Field Verified Points

| OBJECTID	Title	Date_Creat	Description
1	Placemark 1	2019-11-21T15:08:06-06:00	
2	cave and sink hole	2019-11-23T10:19:51-06:00	
3	fox dump cave.	2019-11-23T09:58:54-06:00	air flow. come back to map.
4	investigate 01	2019-11-23T09:08:50-06:00	took photos. hole in loess
5	Placemark 10 sinkhole	2019-11-23T14:10:23-06:00	
6	Placemark 11 sinkhole	2019-11-23T14:11:59-06:00	
7	Placemark 12 sinkhole	2019-11-23T14:12:10-06:00	
8	Placemark 13 cave triple bypass	2019-11-23T14:31:12-06:00	
9	Placemark 14 cave and sinkhole triple bypass	2019-11-23T14:31:22-06:00	
10	Placemark 15 swallow hole	2019-11-24T09:11:16-06:00	
11	Placemark 16 spring	2019-11-24T09:16:21-06:00	
12	Placemark 17 collapsed cave	2019-11-24T09:23:23-06:00	
13	Placemark 18 cave	2019-11-24T09:43:36-06:00	
14	Placemark 19 sinkhole and cave entrance	2019-11-24T09:51:05-06:00	
15	Placemark 2	2019-11-23T09:47:54-06:00	
16	Placemark 20sinkhole	2019-11-24T09:57:14-06:00	
17	Placemark 21 small cave	2019-11-24T10:02:03-06:00	
18	Placemark 22 insurgance	2019-11-24T10:04:09-06:00	
19	Placemark 23 spring 25 ft e of two caves	2019-11-24T10:27:50-06:00	
20	Placemark 24 collapsef cave	2019-11-24T10:30:04-06:00	sample collected from here. carbonate layer large sample
21	Placemark 25 sinkhole	2019-11-24T10:47:31-06:00	
22	Placemark 26 nutcracker cave	2019-11-24T10:55:54-06:00	
23	Placemark 27 sinkhole wpt 32	2019-11-24T10:59:48-06:00	
24	Placemark 28 sinkhole	2019-11-24T11:06:03-06:00	
25	Placemark 29 sinkhole	2019-11-24T11:06:47-06:00	
26	Placemark 30 sweaty balls cave	2019-11-24T11:26:29-06:00	
27	Placemark 31 exit sweaty balls cave	2019-11-24T11:46:10-06:00	
28	Placemark 32 insurg	2019-11-24T11:53:23-06:00	
29	Placemark 33 sinkhole and cave	2019-11-24T12:18:30-06:00	
30	Placemark 34 slot cave	2019-11-24T12:26:53-06:00	
31	Placemark 35 sinkhole	2019-11-24T12:29:02-06:00	
32	Placemark 36 cave	2019-11-24T12:30:35-06:00	
33	Placemark 37 spring And sonkhole	2019-11-24T12:32:51-06:00	
34	Placemark 8 nippewalla samples collected	2019-11-23T12:21:07-06:00	
35	Placemark 9 sinkhole	2019-11-23T14:10:12-06:00	
36	Placemark shhelter cave	2019-11-23T12:11:20-06:00	
37	sinkhole 1 and caves	2019-11-23T10:06:05-06:00	
38	snk2	2019-11-23T10:40:34-06:00	sinkhole and through cave with tube and speleothems

APPENDIX F: Gary K Karst Points

| OBJEC TID	Date	Name	Karst	Elevation	Comments
1	2019-03-31	Monkey Cave	Cave	566	WP 345, Partially Water Filled, weird organisms in water(FHSU Bio Possibility)
2	2019-03-31	CP Cave	Collapsed Cave	559	WP 346
3	2019-03-31	G6 Cave	Cave	562	WP 347, collected 2 samples
4	2019-03-31	Spring	Spring	556	WP 348
5	2019-03-31	Spring	Spring	556	WP349
6	2019-03-31	proto-conduit	proto-conduit	550	WP350
7	2019-03-31	Microkarst	Microkarst	553	WP 351
8	2019-03-31	Dolomite contact	Dolomite Contact	549	WP 352
9	2019-03-31	Conduit/Spring	Conduit/Spring	555	WP 353, Conduit / Spring near gypsum contact?
10	2019-03-31	Microkarst	Microkarst	556	WP 354

APPENDIX G: Raw Sedimentary Thin Section Point Count

Sample	Gypsum	% Gypsum	Gypsum Laths	% Gypsum Laths	Planar Dolomite	% Dolomite	Pore	% Pore	Exc (fracture)
CC-2	0	0	13	13	87	87	0	0	0
CC-1	0	0	18	18	81	81	0	0	1
G6-2	0	0	3	3	97	97	0	0	0
G6-1	33	32	0	0	69	68	0	0	0
POND	15	15	0	0	86	85	0	0	0
YCAR-2	7	7	0	0	93	93	0	0	0
YCAR-1	4	4	0	0	96	96	0	0	0
UN-E	8	8	0	0	92	92	0	0	0
UN	0	0	0	0	107	100	0	0	0
CP-1	2	2	0	0	97	97	1	1	0
CP-2	4	4	0	0	96	96	0	0	0
CP-3	14	14	0	0	83	82	4	4	0
ACG-1	13	13	0	0	88	87	0	0	0
ACG-2	13	13	0	0	87	86	1	1	0
ACG-3	17	17	0	0	83	83	0	0	0
AC-1	3	3	0	0	97	97	0	0	0
352-1	0	0	0	0	100	100	0	0	0
352-2	0	0	0	0	100	100	0	0	0
SC-1	15	15	0	0	85	85	0	0	0
SC-2	3	3	0	0	97	97	0	0	0
SOC-1	1	1	0	0	99	99	0	0	0
SOC-2	0	0	0	0	100	100	0	0	0
MC-2	16	16	0	0	84	84	0	0	0
MC-1	41	41	0	0	59	59	0	0	0
PC-1	2	2	0	0	97	96	2	2	0

APPENDIX H : NDVI for the months studied in 2018

NDVI March 2018

NDVI April 2018
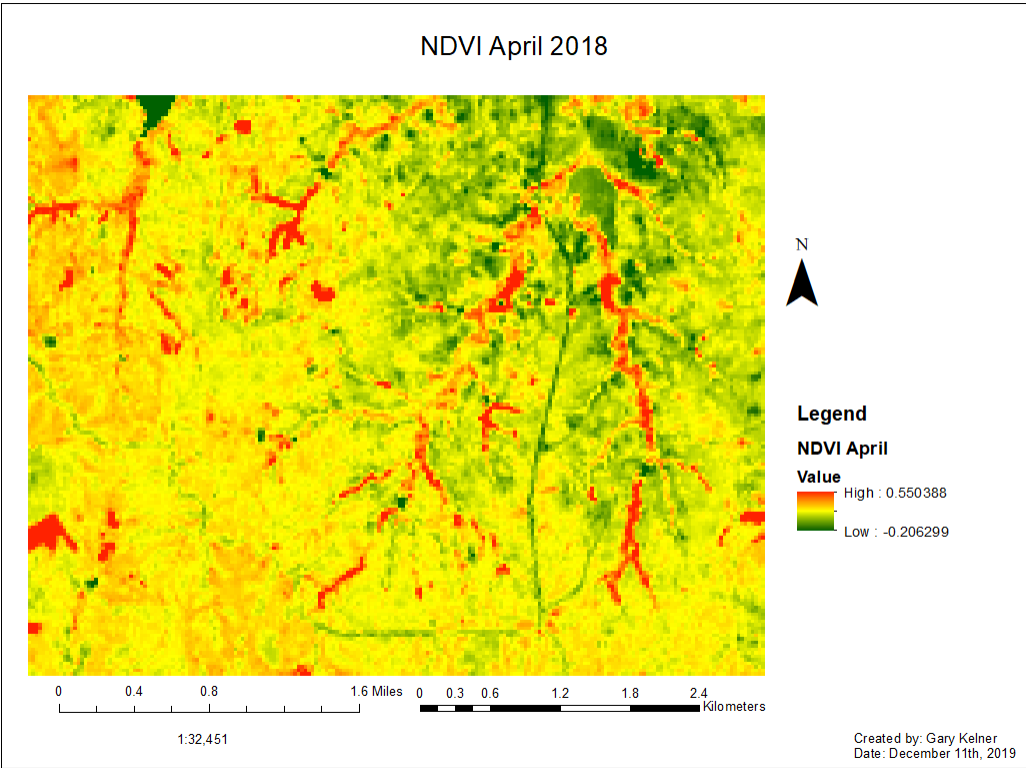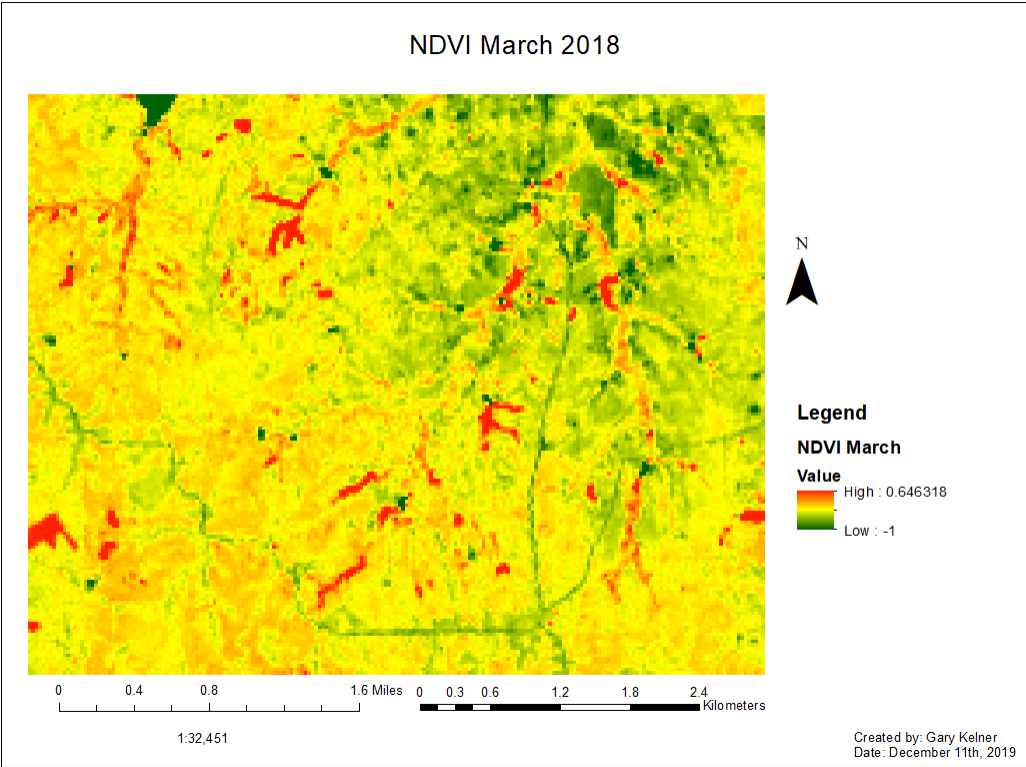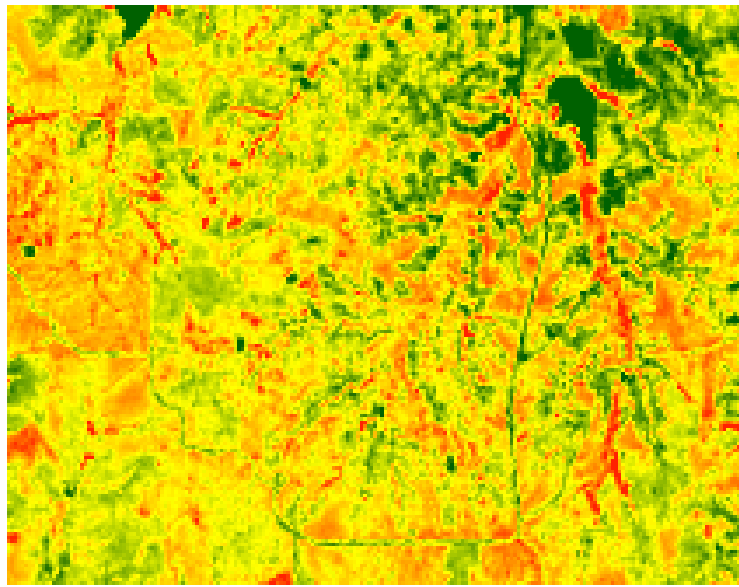
NDVI May 2018

Legend

NDVI May

Value

High : 0.712552

Low : -0.0412169

1:32,451

Created by: Gary Kelner
Date: December 11th, 2019

NDVI August 2018
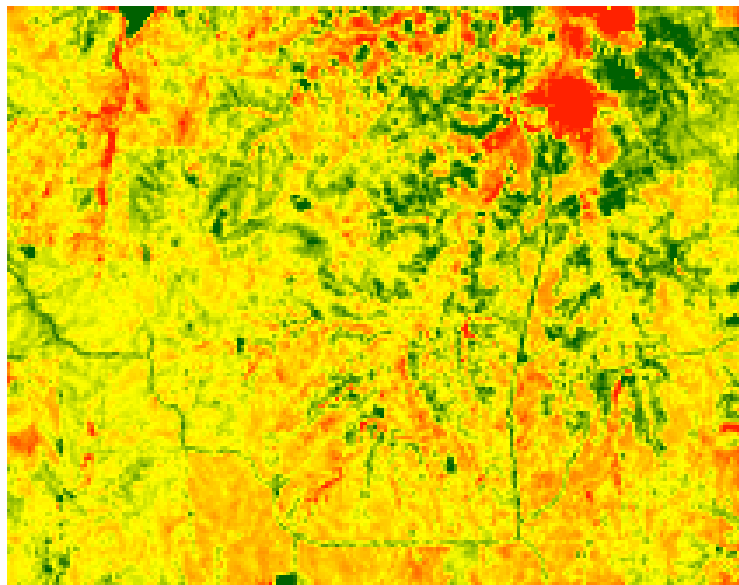
Legend

NDVI August

Value

High : 0.847379

Low : -0.411392

1:32,451

Created by: Gary Kelner
Date: December 11th, 2019

NDVI September 2018
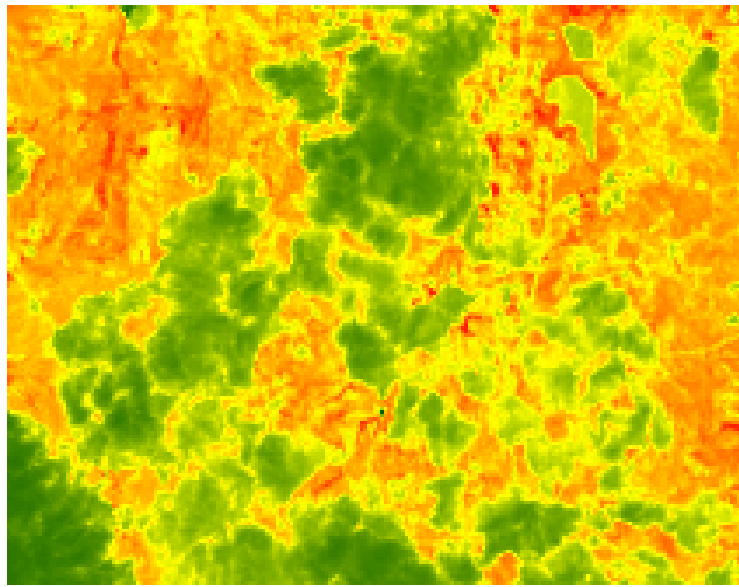

Legend
NDVI September
Value
High : 1
Low : -0.0694864

0   0.4   0.8   1.6 Miles   0 0.3 0.6   1.2   1.8   2.4
Kilometers

1:32,451

Created by: Gary Kelner
Date: December 11th, 2019

NDVI November 2018

Legend
NDVI November
Value
High : 0.741935
Low : -1

0   0.4   0.8   1.6 Miles   0 0.3 0.6   1.2   1.8   2.4
Kilometers

1:32,451

Created by: Gary Kelner
Date: December 11th, 2019

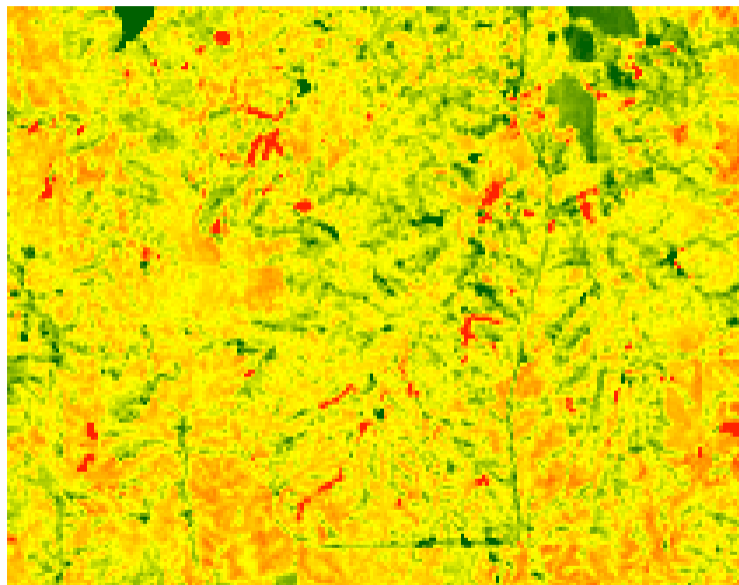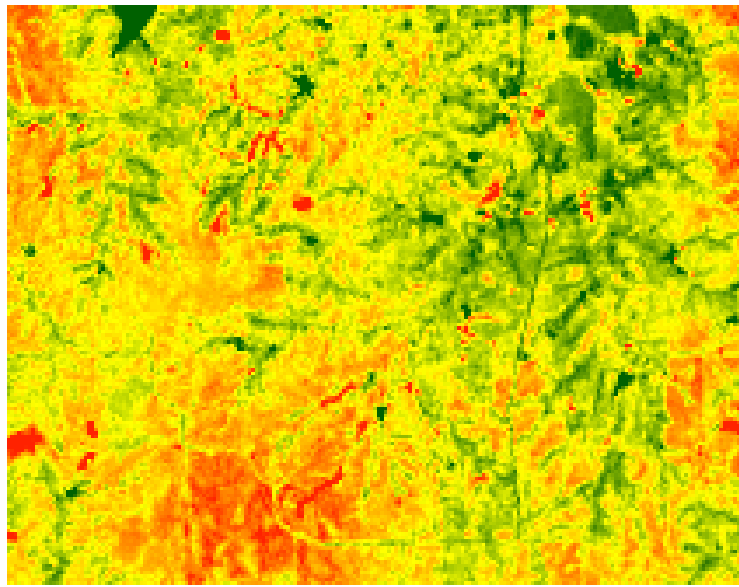# NDVI December 2018

Legend
NDVI December
Value
High : 0.3483

Low : 0.0088249

0   0.4   0.8   1.6 Miles   0   0.3   0.6   1.2   1.8   2.4

Kilometers

1:32,451

Created by: Gary Kelner
Date: December 11th, 2019

Fort Hays State University
FHSU Scholars Repository
Non-Exclusive License Author Agreement

I hereby grant Fort Hays State University an irrevocable, non-exclusive, perpetual license to include my thesis ("the Thesis") in *FHSU Scholars Repository*, FHSU's institutional repository ("the Repository").

I hold the copyright to this document and agree to permit this document to be posted in the Repository, and made available to the public in any format in perpetuity.

I warrant that the posting of the Thesis does not infringe any copyright, nor violate any proprietary rights, nor contains any libelous matter, nor invade the privacy of any person or third party, nor otherwise violate FHSU Scholars Repository policies.

I agree that Fort Hays State University may translate the Thesis to any medium or format for the purpose of preservation and access. In addition, I agree that Fort Hays State University may keep more than one copy of the Thesis for purposes of security, back-up, and preservation.

I agree that authorized readers of the Thesis have the right to use the Thesis for non-commercial, academic purposes, as defined by the "fair use" doctrine of U.S. copyright law, so long as all attributions and copyright statements are retained.

To the fullest extent permitted by law, both during and after the term of this Agreement, I agree to indemnify, defend, and hold harmless Fort Hays State University and its directors, officers, faculty, employees, affiliates, and agents, past or present, against all losses, claims, demands, actions, causes of action, suits, liabilities, damages, expenses, fees and costs (including but not limited to reasonable attorney's fees) arising out of or relating to any actual or alleged misrepresentation or breach of any warranty contained in this Agreement, or any infringement of the Thesis on any third party's patent, trademark, copyright or trade secret.

I understand that once deposited in the Repository, the Thesis may not be removed.

Thesis: A Karst feature Predictability Model Within Barber County, Kansas

Author: Gary M. Kelner

Signature: *Gary M. Kelner*

Date: April 8, 2020